JGR Atmospheres

RESEARCH ARTICLE
10.1029/2019JD030387

Global 3-D Simulations of the Triple Oxygen Isotope Signature $\Delta^{17}O$ in Atmospheric CO_2

Gerbrand Koren[1], Linda Schneider[2,3], Ivar R. van der Velde[4,5], Erik van Schaik[1], Sergey S. Gromov[6,7], Getachew A. Adnew[8], Dorota J. Mrozek Martino[8], Magdalena E. G. Hofmann[8,9], Mao-Chang Liang[10], Sasadhar Mahata[11], Peter Bergamaschi[12], Ingrid T. van der Laan-Luijkx[1], Maarten C. Krol[1,8], Thomas Röckmann[8], and Wouter Peters[1,13]

[1]Meteorology and Air Quality Group, Wageningen University & Research, Wageningen, The Netherlands, [2]Institute of Meteorology and Climate Research (IMK-TRO), Karlsruhe Institute of Technology, Karlsruhe, Germany, [3]Now at Zentrum für Sonnenenergie- und Wasserstoff-Forschung Baden-Württemberg (ZSW), Stuttgart, Germany, [4]Earth System Research Laboratory, National Oceanic and Atmospheric Administration, Boulder, CO, USA, [5]Now at Faculty of Science, VU University Amsterdam, Amsterdam, The Netherlands, [6]Atmospheric Chemistry Department, Max-Planck Institute for Chemistry, Mainz, Germany, [7]Institute of Global Climate and Ecology of Roshydromet and RAS, Moscow, Russia, [8]Institute of Marine and Atmospheric Research, Utrecht University, Utrecht, The Netherlands, [9]Now at Picarro B.V. 's-Hertogenbosch, The Netherlands, [10]Institute of Earth Sciences, Academia Sinica, Taipei, Taiwan, [11]Institute of Global Environmental Change, Xian Jiaotong University, Xian, China, [12]European Commission Joint Research Centre, Ispra (Va), Italy, [13]Centre for Isotope Research, University of Groningen, Groningen, The Netherlands

Key Points:
- This work presents a first view on possible spatial and temporal gradients of $\Delta^{17}O$ in CO_2 across the globe
- Tropical, boreal, and Southern Hemisphere observations of $\Delta^{17}O$ in CO_2 could be of great interest
- We implemented spatially and temporally explicit sources and sinks of $\Delta^{17}O$ in CO_2 in a 3-D model framework

Supporting Information:
- Supporting Information S1

Correspondence to:
G. Koren,
gerbrand.koren@wur.nl

Citation:
Koren, G., Schneider, L., van der Velde, I. R., van Schaik, E., Gromov, S. S., Adnew, G. A., et al. (2019). Global 3-D simulations of the triple oxygen isotope signature $\Delta^{17}O$ in atmospheric CO_2. *Journal of Geophysical Research: Atmospheres*, *124*, 8808–8836. https://doi.org/10.1029/2019JD030387

Received 1 FEB 2019
Accepted 28 MAY 2019
Accepted article online 19 JUN 2019
Published online 4 AUG 2019

Abstract The triple oxygen isotope signature $\Delta^{17}O$ in atmospheric CO_2, also known as its "^{17}O excess," has been proposed as a tracer for gross primary production (the gross uptake of CO_2 by vegetation through photosynthesis). We present the first global 3-D model simulations for $\Delta^{17}O$ in atmospheric CO_2 together with a detailed model description and sensitivity analyses. In our 3-D model framework we include the stratospheric source of $\Delta^{17}O$ in CO_2 and the surface sinks from vegetation, soils, ocean, biomass burning, and fossil fuel combustion. The effect of oxidation of atmospheric CO on $\Delta^{17}O$ in CO_2 is also included in our model. We estimate that the global mean $\Delta^{17}O$ (defined as $\Delta^{17}O = \ln(\delta^{17}O + 1) - \lambda_{RL} \cdot \ln(\delta^{18}O + 1)$ with $\lambda_{RL} = 0.5229$) of CO_2 in the lowest 500 m of the atmosphere is 39.6 per meg, which is ~20 per meg lower than estimates from existing box models. We compare our model results with a measured stratospheric $\Delta^{17}O$ in CO_2 profile from Sodankylä (Finland), which shows good agreement. In addition, we compare our model results with tropospheric measurements of $\Delta^{17}O$ in CO_2 from Göttingen (Germany) and Taipei (Taiwan), which shows some agreement but we also find substantial discrepancies that are subsequently discussed. Finally, we show model results for Zotino (Russia), Mauna Loa (United States), Manaus (Brazil), and South Pole, which we propose as possible locations for future measurements of $\Delta^{17}O$ in tropospheric CO_2 that can help to further increase our understanding of the global budget of $\Delta^{17}O$ in atmospheric CO_2.

1. Introduction

Oxygen has three naturally occurring stable isotopes ^{16}O, ^{17}O, and ^{18}O of which ^{16}O is by far the most abundant on Earth. For atmospheric CO_2, the relative abundances of $C^{16}O^{16}O$, $C^{17}O^{16}O$, and $C^{18}O^{16}O$ are 99.5%, 0.077%, and 0.41%, respectively (see, e.g., Eiler & Schauble, 2004). We can quantify the oxygen isotopic composition of a sample as

$$\delta^n = \frac{\left[{}^nO/{}^{16}O\right]_{sample}}{\left[{}^nO/{}^{16}O\right]_{VSMOW}} - 1, \quad (1)$$

where n refers to the rare oxygen isotope (i.e., $n = 17$ or 18) and Vienna Standard Mean Ocean Water (VSMOW) is used as the reference standard and δ values are usually expressed in per mil (‰). The isotopic composition of oxygen-containing molecules on Earth, like CO_2 or H_2O, is affected by processes such as diffusion, evaporation, and condensation. These processes depend on the mass of the molecules and therefore

result in a mass-dependent fractionation of the oxygen isotopes. As a consequence, the variations in $\delta^{17}O$ and $\delta^{18}O$ of oxygen-containing substances on Earth are strongly correlated.

A deviation from the mass-dependent fractionation can be expressed by the $\Delta^{17}O$ signature ("triple oxygen isotope" or "^{17}O excess"). In this study we consistently use the logarithmic definition for $\Delta^{17}O$ (see Section S1 of the supporting information for an overview of alternative definitions that are commonly used)

$$\Delta^{17}O = \ln(\delta^{17}O + 1) - \lambda_{RL} \cdot \ln(\delta^{18}O + 1), \quad (2)$$

which is usually expressed in per mil (‰) or per meg (0.001‰), depending on the magnitude of the $\Delta^{17}O$ signature, where λ_{RL} is the reference line. We selected $\lambda_{RL} = 0.5229$, which is equal to the isotopic equilibration constant of CO_2 and water $\lambda_{CO_2-H_2O}$ (Barkan & Luz, 2012), since equilibration of CO_2 with water is a key process in our study. As a consequence, the $\Delta^{17}O$ signature of CO_2 that equilibrates with a large amount of water will be reset to the $\Delta^{17}O$ signature of the water reservoir. Relative to this selected reference line λ_{RL}, other mass-dependent processes (e.g., diffusion) result in a minor fractionation of oxygen isotopes (fractionation of $\Delta^{17}O$ due to diffusion is described in section 2.3.1).

Stratospheric CO_2 was shown to be anomalously enriched in oxygen isotopes with $\Delta^{17}O \gg 0‰$ in measurement campaigns performed with rockets (Thiemens et al., 1995a), aircraft (Boering et al., 2004; Thiemens et al., 1995b), balloons (Alexander et al., 2001; Kawagucci et al., 2008; Lämmerzahl et al., 2002; Mrozek et al., 2016), or using aircraft and balloons (Wiegel et al., 2013; Yeung et al., 2009). The anomalous isotopic composition of stratospheric CO_2 has been linked to oxygen exchange with stratospheric O_3, which has a positive $\Delta^{17}O$ signature, by Yung et al. (1991). Photolysis of O_3 produces the highly reactive radical $O(^1D)$

$$O_3 + h\nu \rightarrow O_2 + O(^1D), \quad (3)$$

which can form the unstable CO_3^* when colliding with CO_2, which dissociates into CO_2 and an oxygen radical

$$O(^1D) + CO_2 \rightarrow CO_3^* \rightarrow CO_2 + O(^3P). \quad (4)$$

The oxygen atom that is removed by disintegration of CO_3^* is random (except for the small fractionation of a few per mil favoring ^{18}O remaining in the CO_2 product; Mebel et al., 2004), such that there is an approximately two-thirds probability that the reactions in equations (3) and (4) will result in the substitution of an oxygen atom in CO_2 with an oxygen atom that was originally present in O_3. This exchange of oxygen atoms from stratospheric O_3 to CO_2 is responsible for the transfer of the ^{17}O anomaly (i.e., $\Delta^{17}O \gg 0‰$) from stratospheric O_3 to stratospheric CO_2.

In the upper troposphere, there is an influx of stratospheric CO_2 with $\Delta^{17}O \gg 0‰$ (this stratospheric influence on $\Delta^{17}O$ of tropospheric CO_2 was recently observed by Laskar et al. (2019) in air samples from two aircraft flights). Following transport to the troposphere, the CO_2 is mixed and can come into contact with liquid water in vegetation, soils, or oceans. When CO_2 dissolves in liquid H_2O, exchange of oxygen atoms occurs, such that the CO_2 that is released back to the atmosphere has a signature of $\Delta^{17}O \approx 0‰$. The exchange between CO_2 and H_2O in vegetation is highly effective due to the presence of the enzyme carbonic anhydrase, whereas the exchange of oxygen isotopes between CO_2 and cloud droplets is negligible due to the absence of carbonic anhydrase in the atmosphere (Francey & Tans, 1987). The resulting $\Delta^{17}O$ signature in tropospheric CO_2 reflects a dynamic balance of highly enriched stratospheric CO_2 and equilibration that occurs in vegetation and other water reservoirs. Tropospheric measurements of $\Delta^{17}O$ in CO_2 have previously been performed in Jerusalem, Israel (Barkan & Luz, 2012); La Jolla, United States (Thiemens et al., 2014); Taipei, Taiwan (Liang & Mahata, 2015; Liang et al., 2017a, 2017b; Mahata et al., 2016a), Göttingen, Germany (Hofmann et al., 2017), and Palos Verdes, United States (Liang et al., 2017b).

Gross primary production (GPP; the gross uptake of CO_2 by vegetation through photosynthesis) is a key process in the carbon cycle which is currently poorly constrained. Increasing our understanding of the terrestrial carbon cycle is essential for predicting future climate and atmospheric CO_2 concentrations (Booth et al., 2012). An estimate of 120 PgC/year for global GPP was provided by Beer et al. (2010) by using machine learning techniques to extrapolate a database of eddy covariance measurements of CO_2 to the global domain. An estimate of 150–175 PgC/year for global GPP was derived by Welp et al. (2011) based on the response of

$\delta^{18}O$ in atmospheric CO_2 after El Niño–Southern Oscillation events. The large spread in estimates of global GPP clearly indicates our current lack of understanding of the biospheric domain in the global carbon cycle.

Because the $\Delta^{17}O$ signature of tropospheric CO_2 strongly depends on the magnitude of the exchange of CO_2 with liquid water in leaves, it is a potential tracer for GPP, as was first proposed by Hoag et al. (2005). Similarly, the $\delta^{18}O$ signature of tropospheric CO_2 has been explored to constrain terrestrial carbon fluxes by Ciais et al. (1997a, 1997b), Peylin et al. (1997, 1999), and Cuntz et al. (2003a, 2003b). The main advantage of using $\Delta^{17}O$ instead of $\delta^{18}O$ is that the signal is less affected by processes in the hydrological cycle (e.g., evaporation and condensation), since these are largely mass dependent (Hoag et al., 2005). Besides constraining gross terrestrial CO_2 fluxes, other possible applications of $\Delta^{17}O$ in atmospheric CO_2 have been suggested, such as constraining stratospheric circulation and constraining the abundance and variability of $O(^1D)$ (e.g., Alexander et al., 2001).

The first two-box model for $\Delta^{17}O$ in tropospheric CO_2 for the Northern and Southern Hemispheres was developed by Hoag et al. (2005). This conceptual box model takes into account the exchange fluxes of CO_2 between the troposphere and the stratosphere, vegetation, and oceans. In addition, the supply of CO_2 from fossil fuel combustion and land use change is incorporated in the box model. All these CO_2 fluxes are associated with a reservoir-specific $\Delta^{17}O$ signature. The resulting $\Delta^{17}O$ for tropospheric CO_2 was calculated using a mass balance. Results from Hoag et al. (2005) can be converted into our reference frame, as defined in equation (2), assuming a global $\delta^{18}O$ signature of 41.5‰ (observations from Francey & Tans, 1987, show that the global mean $\delta^{18}O$ in CO_2 is ~0‰ PDB-CO_2, which can be converted using equation 5 from Brenninkmeijer et al. (1983) into 41.5‰ VSMOW), which yields $\Delta^{17}O = 0.066$‰ for tropospheric CO_2.

A more sophisticated global one-box model was developed by Hofmann et al. (2017). This model takes into account that certain processes (e.g., diffusion of CO_2 from the atmosphere into leaf stomata) can fractionate oxygen isotopes and influence the $\Delta^{17}O$ signature of CO_2. Another significant difference with the model from Hoag et al. (2005) is the soil invasion fluxes that are taken into account. Also, both models differ in the magnitude of the CO_2 fluxes and the $\Delta^{17}O$ reservoir signatures. Based on a Monte Carlo simulation where the uncertainty in the input variables is considered, Hofmann et al. (2017) predict $\Delta^{17}O = 0.061 \pm 0.033$‰ for tropospheric CO_2.

In recent years, there have been developments in the available measurement techniques for $\Delta^{17}O$ in CO_2. Mahata et al. (2013, 2016b) developed a measurement technique based on the equilibration between CO_2 and O_2 catalyzed by hot platinum, followed by measurement of the $\Delta^{17}O$ signature of O_2, from which the initial $\Delta^{17}O$ signature of CO_2 can be inferred with a precision of 8 per meg. Barkan and Luz (2012) developed a high-precision measurement technique based on equilibration of CO_2 and H_2O, resulting in a precision of 5 per meg for $\Delta^{17}O$ in CO_2. Using laser-based techniques, Stoltmann et al. (2017) were able to reach a precision for $\Delta^{17}O$ in CO_2 of better than 10 per meg. The quantum cascade laser developed by Aerodyne Research is also able to measure $\Delta^{17}O$ in CO_2 with high precision (McManus et al., 2015; Nelson et al., 2008). In addition, a recently developed ion fragment method allows to measure $\delta^{17}O$ and $\delta^{18}O$ directly on CO_2 without the need of chemical conversion (Adnew et al., 2019). The recent developments in the measurement techniques for $\Delta^{17}O$ in CO_2 are essential for its application as tracer for the terrestrial carbon cycle.

Because of the recent advancements in measurement techniques for $\Delta^{17}O$ in CO_2, it is now possible to observe spatial and temporal gradients of $\Delta^{17}O$ more accurately. To simulate the spatial and temporal variability of the $\Delta^{17}O$ signal in atmospheric CO_2, the available box models are not suitable and a 3-D model framework is required. For this purpose, an oxygen isotope module for atmospheric CO_2 was implemented in the atmospheric transport model TM5 (Huijnen et al., 2010; Krol et al., 2005). Results from an early version of our 3-D model were compared with the $\Delta^{17}O$ measurement series from Göttingen, Germany (Hofmann et al., 2017). A detailed description of our updated $\Delta^{17}O$ model is given in section 2, and the changes in our current model with respect to the earlier version used by Hofmann et al. (2017) are summarized in section S2 of the supporting information. The model results are reported in section 3, followed by the discussion and conclusion in sections 4 and 5.

2. Methods

2.1. General Model Description

Our model framework for $\Delta^{17}O$ in atmospheric CO_2 is based on the atmospheric transport model TM5 (Krol et al., 2005), which is driven by ERA-Interim meteorological fields (Dee et al., 2011) provided by the

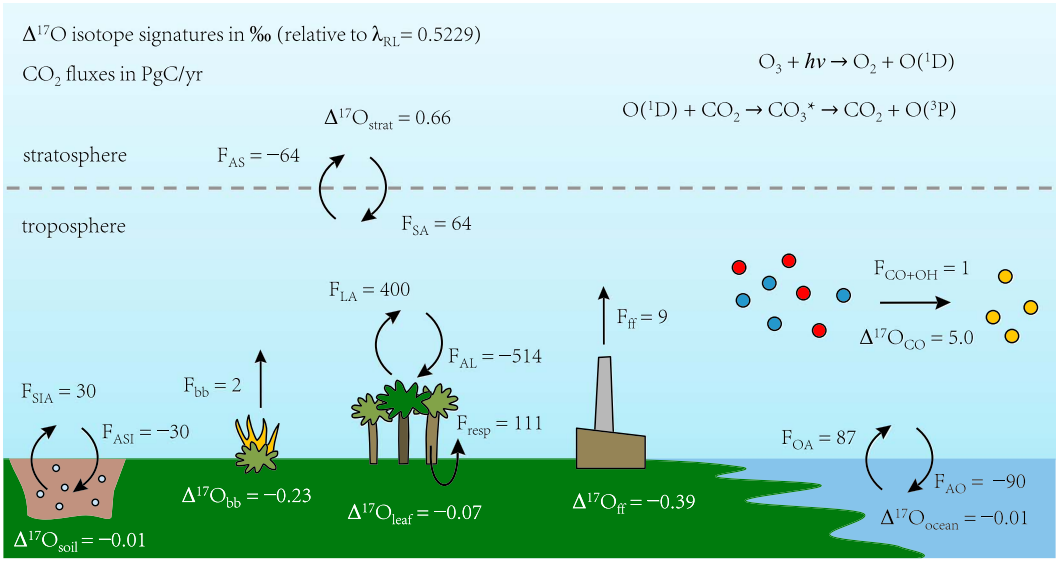

Figure 1. Conceptual overview of processes affecting the $\Delta^{17}O$ signature of atmospheric CO_2 in our model. The CO_2 mass fluxes, indicated with symbol F, are given in units of PgC/year, and $\Delta^{17}O$ signatures are given in ‰ as defined in equation (2) relative to a reference line $\lambda_{RL} = 0.5229$. The reported values for CO_2 mass fluxes are integrated over the global domain, averaged over the years 2012/2013 (as reported in Table S2 of the supporting information) and rounded to integer values. As a sign convention, the CO_2 mass fluxes that tend to increase the tropospheric CO_2 mass are expressed as positive numbers. The main source of $\Delta^{17}O$ in tropospheric CO_2 is exchange with the stratosphere (F_{SA} and F_{AS}), as described in section 2.2. The stratospheric signature $\Delta^{17}O_{strat}$ in our model is time and space dependent, and the indicated value of 0.66‰ is the effective signature that is associated with stratosphere-troposphere exchange (determined from the stratosphere-troposphere CO_2 mass flux and $\Delta^{17}O$ isoflux as reported in Table S2 of the supporting information). The main sink for $\Delta^{17}O$ in tropospheric CO_2 is the exchange with leaves (F_{AL} and F_{LA}), which is associated with a large uncertainty. Also, the magnitude of the exchange fluxes between the soil and atmosphere (F_{ASI} and F_{SIA}) is uncertain. The implementation of the surface sources and sinks of CO_2 is described in section 2.3. Note that the high $\Delta^{17}O_{CO}$ signature is not directly transferred to CO_2 because of fractionation of oxygen isotopes that occurs during the oxidation of CO, as described in section 2.4.

European Centre for Medium-Range Weather Forecasts. TM5 uses a longitude-latitude grid of 6° × 4°, 3° × 2°, or 1° × 1° resolution, depending on the chosen setup. Also, TM5 allows the use of two-way nested zoom regions to simulate with a higher horizontal resolution for specific regions. For the vertical coordinate TM5 uses 25, 34, or 60 hybrid sigma-pressure levels, such that the lowest model levels follow the surface elevation and the higher levels are (almost completely) isobaric. For this study, we performed simulations with the coarsest resolution (i.e., a horizontal resolution of 6° × 4° and 25 vertical levels with the highest model level at 47.8 Pa).

In our model we apply two-way CO_2 fluxes, exchanging between the stratosphere, biosphere, soil, ocean and the troposphere, and one-way CO_2 fluxes from fossil fuel combustion, biomass burning, and oxidation of CO into the troposphere, as illustrated in Figure 1. Modeling the gross two-way exchange fluxes for some reservoirs is necessary to estimate the resulting $\Delta^{17}O$ signature of tropospheric CO_2. The CO_2 fluxes in our model are time and space dependent and can originate from the stratosphere (described in section 2.2), the Earth surface (section 2.3) and are present within the troposphere itself in the case of oxidation of atmospheric CO (section 2.4). Also, the $\Delta^{17}O$ signatures of the different reservoirs are indicated in Figure 1. The $\Delta^{17}O$ signatures for stratospheric CO_2, soil water, leaf water, and atmospheric CO are time and space dependent in our model. Note that for the exchange fluxes between the atmosphere and biosphere, kinetic fractionation affects the $\Delta^{17}O$ signature (described in sections 2.3.1 and 2.3.2) and that the oxidation of CO by OH is not a mass-dependent process, such that the $\Delta^{17}O$ signature of atmospheric CO is not directly transferred to CO_2 (described in more detail in section 2.4).

In our model framework we implemented CO_2 and $C^{17}OO$ as independent tracers, while assuming a fixed atmospheric signature of $\delta^{18}O = 41.5$‰ VSMOW. With the fixed $\delta^{18}O$, we can translate the imposed boundary conditions (i.e., sources and sinks) of $\Delta^{17}O$ into an equivalent boundary condition for the $\delta^{17}O$ signature, based on equation (2). Subsequently, the $C^{17}OO$ tracer mass can be determined from the local tracer mass

Table 1
Overview of the Main Model Parameters and Available Settings for the 3-D $\Delta^{17}O$ Model

Reservoir	Section	Model parameter	Base setting	Alternative settings
Stratosphere	2.2	$\Delta^{17}O$–N_2O fit	Least squares fit	Upper/lower 95% confidence limit fit
		$[N_2O]$ fit threshold	240 ppb level	Zero or positive value
		Relaxation time scale	0 hr (i.e., no relaxation)	Zero or positive value
Vegetation	2.3.1	Soil water $\Delta^{17}O$	Distributed from precipitation	Constant $\Delta^{17}O_{soil}$
		Leaf water $\Delta^{17}O$	Dynamic from rel. humidity	Constant λ_{transp}
Soil	2.3.2	Invasion flux magnitude	30 PgC/year globally	Zero or positive value
		Invasion flux distribution	Scaled from CO_2 respiration flux	Scaled from H_2 deposition velocity
Ocean	2.3.3	CO_2 fluxes	Dynamically coupled to $[CO_2]$	Calculated from predefined $[CO_2]$
		$C^{17}OO$ fluxes	Dynamically coupled to $[C^{17}OO]$	Calculated from predefined $[C^{17}OO]$
Atmospheric CO	2.4	Setting	Not included	Included with nonzero ϵ_{CO+OH}

Note. Note that the soil water signature $\Delta^{17}O_{soil}$ is listed here under the vegetation reservoir, but it also affects the soil invasion fluxes. The model results with base settings are described in sections 3.1.1 and 3.1.2. The effect of some of the alternative settings on the model predictions is discussed in section 3.1.3.

of CO_2 and $\delta^{17}O$ using equation (1). The $C^{17}OO$ tracer mass can then be transported in our atmospheric model. By again using $\delta^{18}O = 41.5‰$ VSMOW, we can "translate" the simulated $C^{17}OO$ tracer mass back into $\Delta^{17}O$ for analysis. By using a fixed $\delta^{18}O$ signature, we are able to simulate the transport of the $\Delta^{17}O$ signature in CO_2, without the need of explicitly modeling the variations in $\delta^{18}O$ that are strongly related to the water cycle (Ciais et al., 1997a, 1997b; Cuntz et al., 2003a, 2003b; Peylin et al., 1997, 1999). The consequence of this approach is that our model simulated $\delta^{17}O$ cannot be directly compared to $\delta^{17}O$ observations. Model output becomes meaningful after converting the simulated $\delta^{17}O$ fields using the fixed $\delta^{18}O$ signature into $\Delta^{17}O$ fields. To convert isotopic signatures to isotope ratios, we use $\left[^{18}O/^{16}O\right]_{VSMOW} = 2005.20 \cdot 10^{-6}$ (Baertschi, 1976) and $\left[^{17}O/^{16}O\right]_{VSMOW} = 379.9 \cdot 10^{-6}$ (Li et al., 1988). Note that more recent studies estimate the latter to be slightly higher, $386.7 \cdot 10^{-6}$ and $382.7 \cdot 10^{-6}$ according to Assonov and Brenninkmeijer (2003) and Kaiser (2008) respectively, but the effect on our simulated $\Delta^{17}O$ is negligible.

We have defined several model parameters that can be set to user-specified values. The motivation for this implementation is that many of the model parameters are uncertain (e.g., the magnitude of the soil invasion flux, as discussed in section 2.3.2), and this flexibility allows us to efficiently investigate the sensitivity to these model parameters. An overview of the most important model parameters and the available settings is given in Table 1. A more detailed explanation of the model parameters and available settings is given in the

Table 2
Overview of Performed Simulations for Sensitivity Analysis Including the Base Model Run

Name	Description
`BASE`	Base model run
`ST_LOWER`	95% confidence interval lower limit fit
`ST_UPPER`	95% confidence interval upper limit fit
`SOIL_CONST`	$\Delta^{17}O_{soil} = -5$ per meg
`LEAF_CONST`	$\lambda_{transp} = 0.5156$
`RESP_240`	Respiration scaling; global magnitude 240 PgC/year
`RESP_450`	Respiration scaling; global magnitude 450 PgC/year
`HYD_240`	H_2 deposition scaling; global magnitude 240 PgC/year
`HYD_450`	H_2 deposition scaling; global magnitude 450 PgC/year
`CO_ROCK`	ϵ_{CO+OH} from Röckmann et al. (1998a)
`CO_FEIL`	ϵ_{CO+OH} from Feilberg et al. (2005)

Note. The resulting $\Delta^{17}O$ signature of atmospheric CO_2 and the $\Delta^{17}O$ isofluxes for the base model run are discussed in sections 3.1.1 and 3.1.2. The results of the sensitivity analyses are given in section 3.1.3.

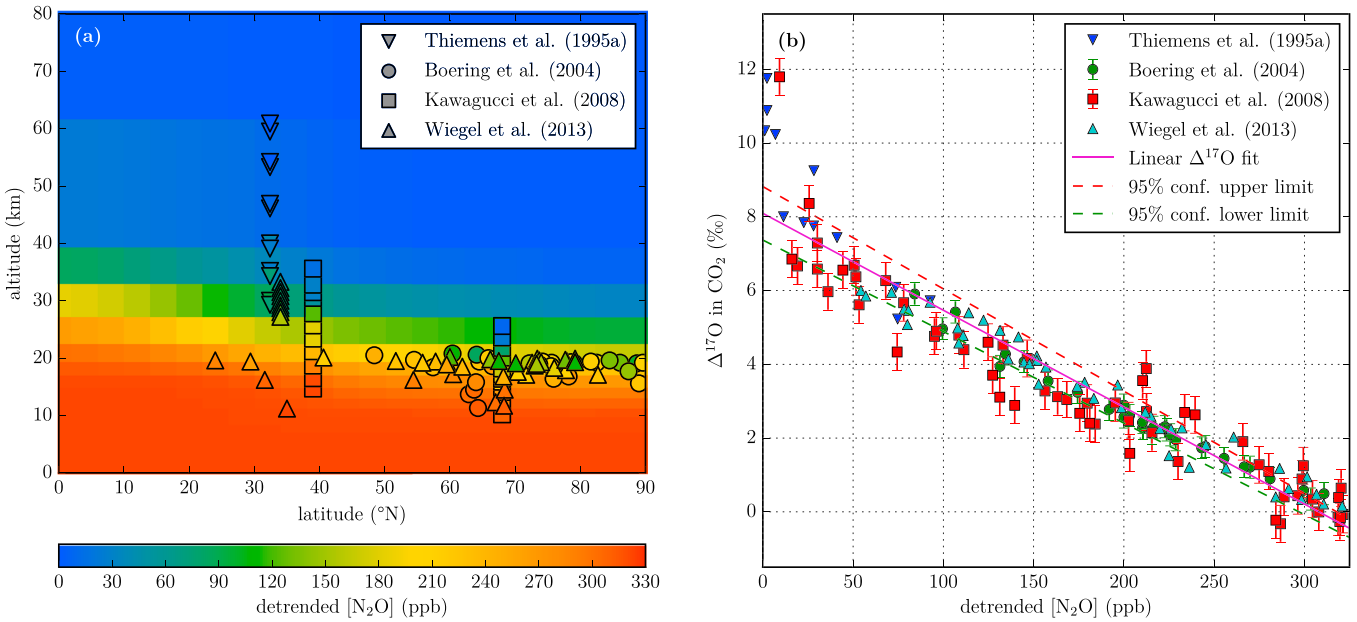

Figure 2. Overview of simulated and measured stratospheric N_2O mole fraction and $\Delta^{17}O$ signature in CO_2. (a) Annual mean, zonal mean TM5 model predictions of detrended N_2O mole fractions using a horizontal resolution of 6° × 4° and 25 vertical levels compared to detrended measurements of N_2O mole fractions from Thiemens et al. (1995a), Boering et al. (2004), Kawagucci et al. (2008), and Wiegel et al. (2013) for stratospheric air in Northern Hemisphere. The background color indicates the value of the TM5 model prediction, and the color of the symbols indicates the measured value. (b) $\Delta^{17}O$ signatures of stratospheric CO_2 versus detrended N_2O mole fraction, constructed from measurements by Thiemens et al. (1995a), Boering et al. (2004), Kawagucci et al. (2008), and Wiegel et al. (2013) and linear least squares fit with its corresponding 95% confidence interval. The error bars from Thiemens et al. (1995a) and Wiegel et al. (2013) are omitted from the figure to improve visibility.

following sections. A summary of the model simulations that were conducted in this research is provided in Table 2.

2.2. Stratospheric Source of $\Delta^{17}O$ in CO_2

2.2.1. N_2O–$\Delta^{17}O(CO_2)$ Correlation

The production of isotopically anomalously enriched CO_2 in the stratosphere has been linked to the exchange of oxygen atoms between O_3 and CO_2 via $O(^1D)$ as described in section 1 and shown in equations (3) and (4). Since the initial discovery of stratospheric CO_2 with $\Delta^{17}O \gg 0‰$, a number of research groups were able to produce anomalously enriched CO_2 from UV-irradiated O_2 or O_3 and CO_2 in controlled laboratory environments (Chakraborty & Bhattacharya, 2003; Johnston et al., 2000; Shaheen et al., 2007; Wen & Thiemens, 1993; Wiegel et al., 2013). Despite the knowledge gained through these studies, there are currently still many questions remaining regarding the dependence on temperature, pressure, photolysis wavelength, and concentrations of O_2, O_3, and CO_2 in the stratosphere. Considering the uncertainties associated with explicitly modeling the production of $\Delta^{17}O$ in CO_2 based on the reactions in equations (3) and (4), we decided to impose $\Delta^{17}O$ in stratospheric CO_2 based on its observed correlation with N_2O, which we expect to be a more robust approach.

The correlation between N_2O and $\Delta^{17}O$ in CO_2 was first used by Luz et al. (1999) to estimate the stratospheric influx of $\Delta^{17}O$ for CO_2 and O_2 into the troposphere. Boering et al. (2004) describe that atmospheric transport is the physical mechanism behind the N_2O–$\Delta^{17}O(CO_2)$ correlation, as both N_2O and $\Delta^{17}O$ in CO_2 are long-lived tracers (the lifetime of N_2O is approximately 120 years; Volk et al., 1997). The negative slope of the N_2O–$\Delta^{17}O(CO_2)$ correlation is explained by the opposite effect of stratospheric photochemistry on N_2O and $\Delta^{17}O$ in CO_2 ($\Delta^{17}O$ in CO_2 is produced from $O(^1D)$ originating from O_3 photolysis, as described in section 1, and N_2O is removed by photolysis and $O(^1D)$, as described in section 2.2.2).

Experimental data sets for stratospheric N_2O and $\Delta^{17}O$ in CO_2 from Thiemens et al. (1995a), Boering et al. (2004), Kawagucci et al. (2008), and Wiegel et al. (2013) were examined to test the robustness of the N_2O–$\Delta^{17}O(CO_2)$ correlation. The $\Delta^{17}O$ values for these studies were recalculated from the reported $\delta^{17}O$ and $\delta^{18}O$ signatures using the definition of $\Delta^{17}O$ as given in equation (2). The N_2O mole fractions were detrended to account for the atmospheric growth rate of N_2O and the difference in date of sample collection,

according to the detrending procedure described in section 2.2.2. The reader is referred to the original works for details on experimental techniques and the associated uncertainties. Despite the difference in date and location of sample collection, there is a strong correlation between the N_2O mole fraction and the $\Delta^{17}O$ signature of CO_2 that is linear for N_2O in the range of 50 to 320 ppb as shown in Figure 2b. In the mesosphere the correlation between N_2O and $\Delta^{17}O$ in CO_2 breaks down as discussed in detail by Mrozek (2017).

We derived a linear fit for the detrended N_2O mole fraction and $\Delta^{17}O$ in CO_2 using a least squares approach with equal weights assigned to each individual measurement (data for $[N_2O] < 50$ ppb was excluded), based on the formulation

$$\Delta^{17}O_{fit} = a \cdot ([N_2O]_{dtd} - 320.84) + b, \tag{5}$$

where $[N_2O]_{dtd}$ is the detrended N_2O mole fraction. In addition to the least squares solution for the coefficients a and b in equation (5), we also constructed a 95% confidence interval, as shown in Figure 2b. The effect of the N_2O–$\Delta^{17}O$ fit on the resulting distribution of $\Delta^{17}O$ in CO_2 is tested by performing different simulations (`BASE`, `ST_UPPER` and `ST_LOWER` as defined in Table 2), the results of which are discussed in section 3.1.3.

In our model framework, the fit in equation (5) is implemented with a cutoff at 0‰, to prevent negative $\Delta^{17}O$ values in the stratosphere. Also, a relaxation time can be specified in the model that determines the strength of the coupling between $\Delta^{17}O$ for stratospheric CO_2 and N_2O mole fractions, such that

$$\Delta^{17}O_{new} = \Delta^{17}O_{fit} + e^{-\Delta t/\tau_{relax}}(\Delta^{17}O_{old} - \Delta^{17}O_{fit}), \tag{6}$$

where Δt is the model time step, τ_{relax} is a user-specified time scale, and $\Delta^{17}O_{new}$ and $\Delta^{17}O_{old}$ refer to $\Delta^{17}O$ signature for the new and old time steps, respectively. In our model, we can apply the fit based on the vertical level (e.g., for cells with atmospheric pressure below 100 hPa) or depending on the local N_2O mole fraction (e.g., for cells with N_2O mole fractions below 280 ppb). The values used for these parameters in the base model run are summarized in Table 1.

2.2.2. N_2O

We simulated N_2O based on stratospheric sinks and optimized surface fluxes from Corazza et al. (2011) and Bergamaschi et al. (2015). The 2-D surface fluxes have a time resolution of 1 month and a horizontal resolution of $6° \times 4°$. The 3-D sink fields have the same time resolution and same horizontal resolution and consist of 25 vertical levels. The N_2O surface fluxes are optimized for the years 2006 and 2007 by Corazza et al. (2011) and Bergamaschi et al. (2015), and we extrapolate the N_2O sources for years outside of this range. The N_2O sinks are climatological fields derived from the ECHAM5/MESSy1 model (Brühl et al., 2007). The sink fields distinguish between N_2O loss caused by $O(^1D)$ (roughly 10% of total loss) and photolysis (roughly 90% of N_2O loss) and have a strong seasonal cycle due to the changing orientation of the Earth with respect to the Sun. The sum of the yearly emissions is on average: ~16 TgN/year, and the imbalance between the sources and sinks is ~3.5 TgN/year, resulting in an increase of the N_2O mass in our model. The global N_2O emission and growth rate are in good agreement with results from Hirsch et al. (2006).

In this study, we are not interested in the atmospheric increase of the N_2O mole fraction over time but its correlation with $\Delta^{17}O$ in CO_2. Assonov et al. (2013) have encountered the same issue and constructed a detrending method based on measured N_2O at Mauna Loa. This detrending method assumes a constant growth rate for N_2O mole fractions of $\alpha_{ref} = 0.844 \pm 0.001$ ppb/year, which is representative of tropospheric air but not suitable to the (upper) stratospheric air that we also consider in this study (e.g., upper stratospheric air samples from Thiemens et al. (1995a) with N_2O mole fractions of less than 10 ppb). We modified the detrending method from Assonov et al. (2013) as described in section S3 of the supporting information to arrive at

$$X_{dtd} = X_{obs} \cdot \left[1 - \frac{\alpha_{ref}}{X_{ref}} \cdot (t_{ref} - t_{obs})\right]^{-1}, \tag{7}$$

where X_{obs} and X_{dtd} refer to the observed and detrended mole fractions and where t_{obs} and t_{ref} are, respectively, the time of observation and the reference time (1 January 2007) on which the N_2O mole fractions are projected. This detrending scheme is applied for (1) the validation of the N_2O simulation against N_2O observations, (2) the derivation of the N_2O–$\Delta^{17}O$ fit, and (3) the detrending of simulated stratospheric N_2O before applying the correlation in TM5.

The modeled tropospheric N_2O mole fraction is nearly constant (well mixed) at ~320 ppb (for 1 January 2007), and the NH mole fraction is roughly 0.7–1 ppb higher than for the SH, which agrees well with the results from Hirsch et al. (2006). To test the uncertainty that is associated with our modeled N_2O, we compare our model predictions for N_2O with stratospheric measurements of N_2O. Figure 2a shows a comparison of modeled zonal mean, yearly mean N_2O with detrended experimental data from Thiemens et al. (1995a), Boering et al. (2004), Kawagucci et al. (2008), and Wiegel et al. (2013). For the measurements from Thiemens et al. (1995a), we assume that the latitude of measurements is equal to latitude of the launching site of the rocket. Our model prediction agrees well with the vertical profile from Kawagucci et al. (2008) at 39°N but overestimates the N_2O mole fractions in the upper part of the vertical profile at 68°N. In Figure S1 of the supporting information we provide similar plots for each season.

2.2.3. Stratosphere-Troposphere Exchange

The transport of air masses in our model, including stratosphere-troposphere exchange (STE), is fully driven by the European Centre for Medium-Range Weather Forecasts ERA-Interim meteorological fields (Dee et al., 2011). Since STE is essential in this study, both for the transport of N_2O and for CO_2 with anomalous $\Delta^{17}O$, we aim to diagnose the magnitude and variability of STE. The diagnosed spatiotemporal variation of STE could help to explain variations in predicted $\Delta^{17}O$ in the troposphere.

To diagnose the STE of CO_2 in TM5, two artificial tracers were defined: `CO2_trop` and `CO2_strat` that have the same properties as the normal tracer `CO2` but do not have any sources or sinks at the surface. For each time step, the tracer mass and tracer mass slopes of `CO2_trop` in tropospheric cells are copied from `CO2`, whereas the tracer mass and slopes of `CO2_trop` are set equal to zero for all stratospheric cells. The opposite procedure is performed each time step for the tracer `CO2_strat` after which all tracers in the model are transported. By diagnosing the tracer mass of `CO2_trop` that was transported into the stratosphere, we can determine for each time step a 2-D field of the transport across the user-defined tropopause. By combining the two gross exchange fluxes from `CO2_trop` and `CO2_strat`, we can calculate the net STE flux. This method allows the use of a static flat "tropopause" or a dynamic tropopause derived from the local temperature profile or the local N_2O mole fraction. The transport of $C^{17}OO$ is tracked in a similar fashion, which allows for the calculation of the $\Delta^{17}O$ stratospheric isoflux. Finally, we can determine the troposphere-stratosphere flux F_{AS} by integrating over the tropical region (30°S to 30°N) and the stratosphere-troposphere flux F_{SA} by integrating over the extratropical regions (outside the range 30°S to 30°N).

It is known that meteorological fields from data assimilation systems have the tendency to overestimate the Brewer-Dobson circulation (Bregman et al., 2006; van Noije et al., 2004). The ERA-Interim reanalysis performs better at simulating the Brewer-Dobson circulation than its predecessor ERA-40 (Monge-Sanz et al., 2007), but upward transport is still too large compared to observations (Schoeberl et al., 2008). Also, the advection scheme for transport of tracer mass has an effect on the STE. Bönisch et al. (2008) showed that the "second-order moments" scheme (Prather, 1986) is more accurate for stratospheric transport than the "slopes" scheme by Russell and Lerner (1981) that is used in our current model framework.

Given the importance of STE for our purposes and the difficulty of accurately modeling STE, we compared our diagnosed STE with data from Appenzeller et al. (1996) and Holton (1990). These studies were also used by Luz et al. (1999) to calculate the stratospheric source of $\Delta^{17}O$ for tropospheric CO_2 and O_2 and in the box models by Hoag et al. (2005) and Hofmann et al. (2017). In order to determine the air mass flux crossing the tropopause, we switched off the CO_2 sources and sinks at the surface and initialized the CO_2 tracer with a constant mixing ratio throughout the entire domain. Using our method to track the STE of CO_2 and the imposed constant CO_2 mixing ratio, we inferred the air mass STE. The comparison of our derived STE and data from Appenzeller et al. (1996) and Holton (1990) is shown in Figure 3. It should be noted that the pressure levels for which the fluxes are given are not equal and also the years are different (as indicated in the legend). Still, some general conclusions about the STE in TM5 can be made. The magnitude of the STE from TM5 is for most months in between the estimates from Appenzeller et al. (1996) and Holton (1990) and the timing of the seasonality in STE agrees well. Despite the agreement, it should be noted that the range of reported values by Appenzeller et al. (1996) and Holton (1990) is large, and hence, considerable uncertainty is associated with our model derived STE. The implications of the large uncertainty in STE on the potential application of $\Delta^{17}O$ in CO_2 as tracer of GPP are further discussed in section 4.3.

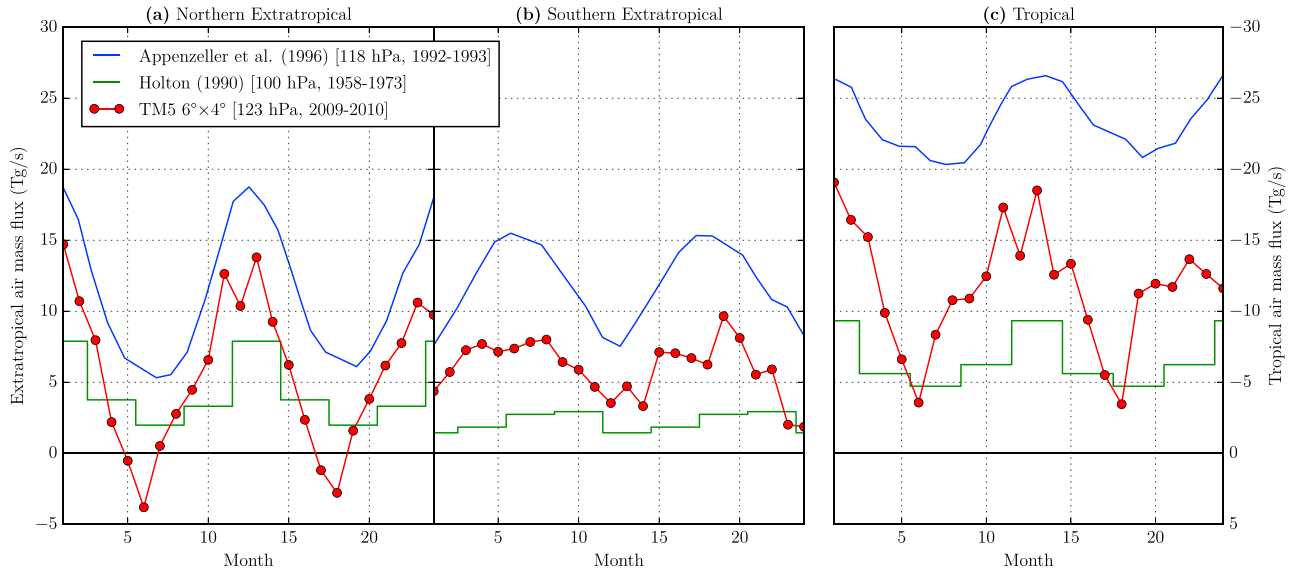

Figure 3. Net air mass flux through ~100-hPa pressure levels from TM5 model simulation and from literature for two consecutive years. Mass fluxes from Appenzeller et al. (1996) for years 1992–1993 are given for the 118-hPa surface. Mass fluxes from Holton (1990) are averaged over years 1958–1973; this averaged data are shown for the first years and are repeated for the second year. Monthly output was taken from our TM5 model simulation; the predicted mass flux is given for 123 hPa for years 2009 and 2010. (a) Fluxes for northern extratropical region (latitudes above 30°N). (b) Fluxes for southern extratropical region (latitudes below 30°S). (c) Fluxes for tropical region (latitudes between 30°N and 30°S). Note that for the tropical mass flux the vertical axis is shown on the right-hand side of the figure and is reversed to facilitate easy visual comparison with the extratropical regions.

The mass fluxes from Appenzeller et al. (1996) are derived from the U.K. Meteorological Office data set (Swinbank & O'Neill, 1994) with a resolution of 3.75° longitude by 2.5° latitude and with a vertical resolution of ~50 hPa in the lowermost stratosphere. We reproduced the STE graph by carefully extracting data points from the graphs in Appenzeller et al. (1996). STE mass fluxes by Holton (1990) are derived from climatological data of Oort (1983) specified on 5° latitude intervals and aggregated for the different seasons. Our TM5 simulation was performed with a horizontal resolution of 6° × 4° and for 25 vertical levels. The TM5 model uses hybrid sigma-pressure levels; for the level at which the mass flux is diagnosed, the levels are almost completely isobaric.

2.3. Surface Sinks of $\Delta^{17}O$ in CO_2

2.3.1. Atmosphere-Leaf Exchange

The atmosphere-leaf exchange of CO_2 is modeled using the Simple Biosphere/Carnegie-Ames-Stanford Approach (SiBCASA) model (Schaefer et al., 2008). To calculate photosynthesis, SiBCASA combines the C_3 and C_4 assimilation models (Collatz et al., 1992; Farquhar et al., 1980) with the Ball-Berry-Collatz stomatal conductance model (Collatz et al., 1991), from which the internal leaf CO_2 concentration c_i can be calculated. SiBCASA is driven by ERA-Interim meteorology with 3-hourly time resolution and a spatial resolution of 1° × 1°. Furthermore, the spatial distribution of C_3 and C_4 vegetation is taken from Still et al. (2003) and SiBCASA uses a climatological mean seasonal leaf phenology based on satellite-derived Normalized Difference Vegetation Index. SiBCASA results are first stored in full resolution in files that are subsequently read by our atmospheric transport model TM5.

The gross atmosphere-leaf exchange fluxes can be derived from the ratio of leaf internal to atmospheric CO_2 concentration c_i/c_a and the assimilation flux F_A (which we obtain by scaling GPP with a factor 0.88, to take out the component that is released through autotrophic leaf respiration, similar to Ciais et al., 1997a), according to

$$F_{AL} = F_A \frac{c_a}{c_a - c_i}, \quad F_{LA} = -F_A \frac{c_i}{c_a - c_i}. \tag{8}$$

We have used monthly averaged GPP-weighted c_i/c_a ratios, similar to Ciais et al. (1997a, 1997b) and Peylin et al. (1997, 1999). Furthermore, our assimilation flux has 3-hourly time resolution, whereas we assume that leaf respiration is a constant fraction of GPP. In future studies we recommend to include c_i/c_a and leaf

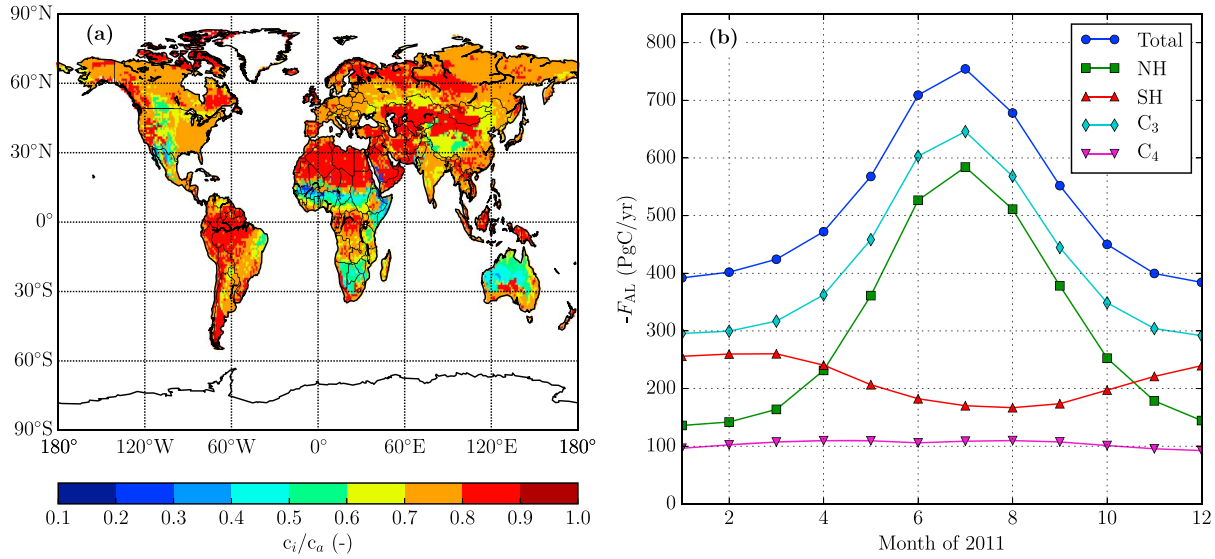

Figure 4. Vegetation parameters as predicted by Simple Biosphere/Carnegie-Ames-Stanford Approach (SiBCASA). (a) Spatial distribution of gross primary production weighted c_i/c_a over the Earth surface averaged over the year 2011. (b) Temporal variation of global atmosphere-leaf flux F_{AL} as predicted by SiBCASA, partitioned over Northern Hemisphere (NH)/Southern Hemisphere (SH) and for C_3/C_4 vegetation.

respiration at the same temporal resolution as GPP, similar to the model by Cuntz et al. (2003a, 2003b) for $\delta^{18}O$ in CO_2, as is also discussed in section 4.1.

In our model framework, we use the sign convention that positive fluxes increase the CO_2 mass in the troposphere. The magnitude of global GPP in our model is taken from SiBCASA and is −133 PgC/year for 2011. This represents a larger uptake than the values of −100 and −120 PgC/year as used in the box models by Hoag et al. (2005) and Hofmann et al. (2017), respectively.

The average distribution of GPP-weighted c_i/c_a for 2011 and the resulting gross atmosphere-leaf flux F_{AL} are shown in Figure 4. The presence of C_4 vegetation in tropical Africa can be recognized clearly by the band of relatively low c_i/c_a ratios near the equator. Our c_i/c_a ratios are higher than what was used in the box models by Hofmann et al. (2017) (a fixed ratio of 0.7) and Hoag et al. (2005) (two thirds and one third for C_3 and C_4 vegetation, respectively, based on a study by Pearcy & Ehleringer, 1984). To prevent excessive atmosphere leaf fluxes in our model, we have imposed an upper limit such that $c_i/c_a \leq 0.9$ for all grid cells in the domain during all months of the simulation. Our global gross atmosphere-leaf fluxes in Figure 4b exhibit a clear seasonal signal, peaking during the NH summer months. During the entire year, our atmosphere-leaf flux is larger than the estimated −352 PgC/year from the box model by Hofmann et al. (2017), which can be explained by our higher c_i/c_a ratios and the larger magnitude of our assimilation flux F_A.

A fraction of the CO_2 that diffuses out of the leaf has equilibrated with leaf water inside the leaf. This can be expressed by dividing the gross leaf-atmosphere flux F_{AL} into an equilibrated and nonequilibrated part

$$F_{LAeq} = (f_{C_3} \cdot \theta_{C_3} + f_{C_4} \cdot \theta_{C_4}) \cdot F_{LA}, \tag{9}$$

$$F_{LAnoneq} = \left(f_{C_3} \cdot [1 - \theta_{C_3}] + f_{C_4} \cdot [1 - \theta_{C_4}]\right) \cdot F_{LA}, \tag{10}$$

where f_{C_i} refers to the fraction of a vegetation type and θ_{C_i} is the vegetation type-specific equilibration constant. In our model we use $\theta_{C_3} = 0.93$ and $\theta_{C_4} = 0.38$ (Gillon & Yakir, 2000, 2001).

The isotopic signature associated with the gross atmosphere-leaf exchange fluxes is determined by the signature of the source (atmospheric CO_2 for F_{AL} and $F_{LAnoneq}$ and leaf water for F_{LAeq}) and kinetic fractionation during inflow and outflow of CO_2 through the leaf stomata

$$\Delta^{17}O_{AL} = \Delta^{17}O_A + (\lambda_{kinetic} - \lambda_{RL}) \cdot \ln(\alpha_{leaf}), \tag{11}$$

$$\Delta^{17}O_{LAeq} = \Delta^{17}O_{leaf} + (\lambda_{kinetic} - \lambda_{RL}) \cdot \ln(\alpha_{leaf}), \tag{12}$$

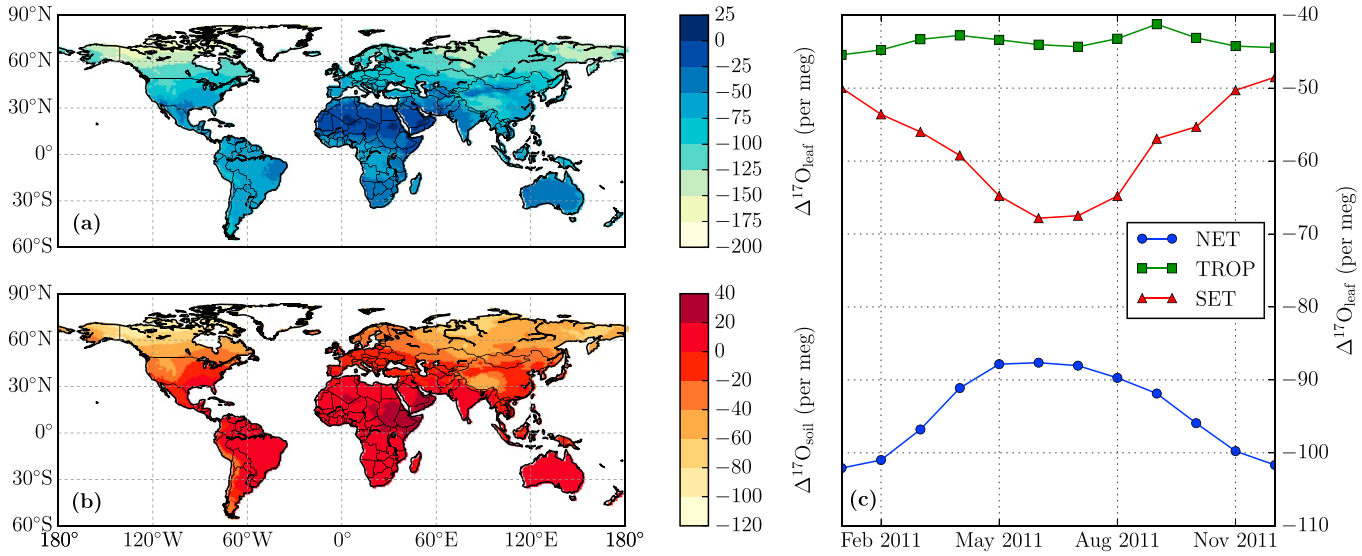

Figure 5. $\Delta^{17}O$ signature of soil water and leaf water. (a) Annual mean distribution of $\Delta^{17}O_{leaf}$ for 2011. (b) Annual mean distribution of $\Delta^{17}O_{soil}$ for 2011. (c) Temporal variation of $\Delta^{17}O_{leaf}$ for northern extratropical region (NET; latitudes above 30°N), tropical region (TROP; latitudes between 30°S and 30°N), and southern extratropical region (SET; latitudes below 30°S) during 2011.

$$\Delta^{17}O_{LAnoneq} = \Delta^{17}O_A + (\lambda_{kinetic} - \lambda_{RL}) \cdot \ln(\alpha_{leaf}), \tag{13}$$

where $\Delta^{17}O_A$ and $\Delta^{17}O_{leaf}$ are the $\Delta^{17}O$ signatures for atmospheric CO_2 and for CO_2 that has equilibrated with leaf water, $\alpha_{leaf} = 0.9926$ is the fractionation factor for diffusion of $C^{18}OO$ relative to CO_2 through leaf stomata (Farquhar et al., 1993), and $\lambda_{kinetic} = 0.509$ is the coefficient associated with kinetic fractionation of $C^{17}OO$ relative to $C^{18}OO$ (Young et al., 2002). A derivation and process-based interpretation of equation (11) is given in section S4 of the supporting information. An alternative derivation for equations (11)–(13) is given in section S5 of the supporting information.

To calculate $\Delta^{17}O_{leaf}$, we first need to determine the isotopic signature of soil water $\Delta^{17}O_{soil}$. We derive the $\delta^{18}O$ signature of soil water from the $\delta^{18}O$ signature of precipitation water, which we obtained from Bowen and Revenaugh (2003) through the portal http://www.waterisotopes.org. We use the yearly average precipitation water signatures, since the amplitude in the seasonal signal of soil water is weaker than for precipitation water and the phase of the seasonal signal can be shifted depending on the depth of the soil water in the soil layer (e.g., Affolter et al., 2015). Similar to Hofmann et al. (2017), we derive the $\Delta^{17}O$ signature of soil water from its $\delta^{18}O$ signature by assuming that soil water falls on the Global Meteoric Water Line, that is,

$$\ln(\delta^{17}O_{soil} + 1) = \lambda_{GMWL} \cdot \ln(\delta^{18}O_{soil} + 1) + \gamma_{GMWL}, \tag{14}$$

with $\lambda_{GMWL} = 0.528$ and $\gamma_{GMWL} = 0.033‰$ (Luz & Barkan, 2010). The resulting distribution of the $\Delta^{17}O_{soil}$ has a maximum value near the equator and drops to its minimum close to the North Pole; see Figure 5b.

The isotopic signature of leaf water $\Delta^{17}O_{leaf}$ (note that we use the same symbol for the $\Delta^{17}O$ signature of CO_2 that has equilibrated with leaf water, because for our selected reference level λ_{RL} these two signatures have the same value) is determined from the isotopic signature of soil water $\Delta^{17}O_{soil}$ and the fractionation occurring due to the transpiration of water

$$\Delta^{17}O_{leaf} = \Delta^{17}O_{soil} + (\lambda_{transp} - \lambda_{RL}) \cdot \ln(\alpha_{transp}), \tag{15}$$

where $\alpha_{transp} = 1/0.9917$ (West et al., 2008) is the fractionation factor of transpiration of $H_2^{18}O$ relative to $H_2^{16}O$ and λ_{transp} is the exponent relating fractionation of $H_2^{17}O$ to transpiration of $H_2^{18}O$

$$\lambda_{transp} = 0.522 - 0.008 \cdot h, \text{for } 0.3 \le h \le 1, \tag{16}$$

where h is the relative humidity as was demonstrated by Landais et al. (2006). The resulting spatial distribution and temporal variation of $\Delta^{17}O_{leaf}$ is shown in Figure 5, where we used relative humidity data from ERA-Interim. The isotopic signature $\Delta^{17}O_{leaf}$ attains its maximum in the African Sahara, where relative humidity is low, and has low values in the arctic region. The leaf signature for the northern and southern extratropical regions (NET and SET) exhibits a seasonal cycle of opposite phase with a peak-to-peak amplitude of ~20 per meg. The $\Delta^{17}O_{leaf}$ in the tropical region has hardly any seasonality.

To test the effect of the soil water signature $\Delta^{17}O_{soil}$ and the leaf water signature $\Delta^{17}O_{leaf}$ on $\Delta^{17}O$ in CO_2, we performed simulations with a spatially distributed $\Delta^{17}O_{soil}$ and temporally and spatially distributed $\Delta^{17}O_{leaf}$ (`BASE` in Table 2) as well as a simulation with a constant soil water signature of −5 per meg (`SOIL_CONST`) and a simulation with a constant relative humidity of 0.8, which can be converted using equation (16) to $\lambda_{transp} = 0.5156$ (`LEAF_CONST`). The results of these simulations are given in section 3.1.3.

2.3.2. Respiration and Soil Invasion

The CO_2 respiration flux is calculated in SiBCASA from multiple above and below ground carbon pools with different turnover rates, depending on temperature and moisture (Schaefer et al., 2008). The calculated respiration flux from SiBCASA is aggregated over a period of 1 month for each 1° × 1° grid cell. From the monthly respiration fluxes and the ERA-Interim 2-m temperature, the coefficient R_0 is determined (see equation (17) for its definition) and stored in a file. In our TM5 model, the CO_2 respiration flux depends on temperature (and thus also on time) according to the following Q_{10} relation (Potter et al., 1993)

$$F_{resp} = R_0 \cdot Q_{10}^{\frac{T-T_{ref}}{10}}, \tag{17}$$

with $Q_{10} = 1.5$ and $T_{ref} = 273.5$ K. For T we used the 2-m temperature from ERA-Interim, which has a spatial resolution of 1° × 1° and a 3-hourly time resolution, which allows us to simulate a diurnal cycle in the respiration flux. The coefficient R_0 is read from the SiBCASA output file and assures that the aggregated monthly respiration flux calculated according to equation (17) agrees with the monthly respiration flux for each cell from SiBCASA. The global respiration flux that we determine with SiBCASA for 2011 is 129 PgC/year (total respiration, including autotrophic leaf respiration).

The isotopic signature of respired CO_2 (excluding the autotrophic leaf respired component, calculated similar to the net assimilation flux as described in section 2.3.1) is determined by equilibration with soil water, followed by kinetic fractionation due to diffusion through the soil column into the atmosphere

$$\Delta^{17}O_{resp} = \Delta^{17}O_{soil} + (\lambda_{kinetic} - \lambda_{RL}) \cdot \ln(\alpha_{soil}), \tag{18}$$

where $\alpha_{soil} = 0.9928$ is the kinetic fractionation factor of $C^{18}OO$ relative to CO_2 for diffusion out of the soil column into the atmosphere (Miller et al., 1999).

The reported magnitudes of the global soil invasion flux cover a wide range: from 30 PgC/year (Stern et al., 2001) to 450 PgC/year (Wingate et al., 2009). The high soil invasion flux estimate is explained by the presence of the enzyme carbonic anhydrase in soils (Wingate et al., 2009). Similar to CO_2, soil invasion fluxes of carbonyl sulfide (COS) are also affected by carbonic anhydrase (Ogée et al., 2016). The soil uptake of COS has been modeled by Launois et al. (2015) assuming that COS uptake scales linearly with v_{dep}, the deposition velocity of molecular hydrogen to soils (based on the assumption that both processes are affected by similar soil microorganisms).

In this study, the global magnitude of the soil invasion flux is set to 30 PgC/year by default (normalized for years 2012–2013) but can be changed to any user-specified value. Also, the spatial distribution of the soil invasion flux can be scaled with the biosphere CO_2 respiration flux (i.e., $F_{SIA} \propto F_{resp}$) or alternatively the hydrogen deposition velocity (i.e., $F_{SIA} \propto v_{dep}$). See Table 1 for an overview of the available model settings for the soil invasion flux. To test the sensitivity of the $\Delta^{17}O$ signature of atmospheric CO_2 on the magnitude and spatial distribution of the soil invasion flux, we performed four additional simulations (`RESP_240`, `RESP_450`, `HYD_240`, and `HYD_450` that are summarized in Table 2), for which the results are discussed in section 3.1.3.

The isotopic signature of CO_2 that diffuses into soils ("ASI") is determined from the local atmospheric $\Delta^{17}O$ as predicted by our model. The $\Delta^{17}O$ signature of CO_2 released from the soil ("SIA") is set equal to the signature of soil water $\Delta^{17}O_{soil}$ described in section 2.3.1. Isotopic fractionation is not taken into account for the soil invasion fluxes, since the ingoing and outgoing fluxes have equal magnitude in our model (i.e., $F_{SIA} = -F_{ASI}$), and therefore, the kinetic fractionation effect on the atmospheric $\Delta^{17}O$ budget cancels out.

2.3.3. Ocean Exchange

The exchange of CO_2 between the atmosphere and the ocean is based on the relationship between wind speed and gas exchange over the ocean as reported by Wanninkhof (1992). The gas transfer coefficient k, in centimeter per hour, is calculated from

$$k = 0.31 \cdot u^2 \cdot \left[\frac{\mathrm{Sc}}{660}\right]^{-0.5}, \tag{19}$$

where u is the wind speed in meter per second and Sc is the dimensionless Schmidt number. Note that the coefficient 0.31 in equation (19) is not dimensionless. Now, the two-way CO_2 exchange fluxes can be determined from

$$F_{\mathrm{AO}} = k \cdot s \cdot p_{\mathrm{CO_2}}, \quad F_{\mathrm{OA}} = k \cdot s \cdot (p_{\mathrm{CO_2}} + \Delta p_{\mathrm{CO_2}}), \tag{20}$$

where s is the solubility of CO_2 in ocean water expressed in mol per cubic meter per atmosphere, $p_{\mathrm{CO_2}}$ is the partial pressure of CO_2 in the atmosphere in unit μ atmosphere (≈0.1 Pa), and $\Delta p_{\mathrm{CO_2}}$ is the CO_2 partial pressure difference between the ocean and the atmosphere in unit μ atmosphere. When we express k in meter per second, the CO_2 fluxes have units of mol per squared meter per second. For cells that are covered with sea ice, the exchange fluxes are set to zero. The sea ice cover and wind speed data are taken from the ERA-Interim data set (Dee et al., 2011), with a time resolution of 3 hr and a horizontal resolution of 1° × 1°. Data for solubility, CO_2 partial pressure difference, and the Schmidt number are taken from Jacobson et al. (2007) with a horizontal resolution of 5° × 4° and a temporal resolution of 1 month.

The isotopic signature of ocean water is taken as $\Delta^{17}O_{\mathrm{ocean}} = -0.005‰$ (Luz & Barkan, 2010). Note that equilibration between CO_2 and H_2O does not result in a fractionation of our $\Delta^{17}O$ signal, because we have taken the CO_2–H_2O equilibration constant as our reference line (i.e., $\lambda_{\mathrm{RL}} = \lambda_{\mathrm{CO_2-H_2O}}$). We have neglected the kinetic fractionation effect for diffusion across the ocean-atmosphere interface, since the associated fractionation factor for $C^{18}OO$ relative to CO_2 is close to 1 ($\alpha_{\mathrm{ocean}} \approx 0.9992$ according to Vogel et al., 1970) and the gross ocean fluxes largely cancel out (with a difference of ~3 PgC/year on the global scale; see Figure 1).

In our model, the ocean sink for the CO_2 and $C^{17}OO$ tracers can be determined from predefined constant CO_2 and $C^{17}OO$ concentrations or dynamically coupled to the local concentrations of CO_2 and $C^{17}OO$ above the ocean surface that the model calculates each time step (see Table 1 for an overview of the available model settings). For the results that we include in this paper, we always used the dynamic coupling between the ocean sink and the local atmospheric concentration.

2.3.4. Fossil Fuel Combustion and Biomass Burning

The CO_2 fluxes from fossil combustion in our model are based on the Emissions Database for Global Atmospheric Research (EDGAR) version 4.2 from the Joint Research Centre of the European Union. The temporal resolution of this data set was improved by coupling to country and sector-specific time profiles by the Institute for Energy Economics and the Rational Use of Energy from the University of Stuttgart. For our model we use the CO_2 fluxes with a monthly time resolution and a horizontal resolution of 1° × 1°. We assign a signature of $\Delta^{17}O_{\mathrm{ff}} = -0.386‰$ to the CO_2 that is released by fossil fuel combustion, which is largely determined by the $\Delta^{17}O$ signature of ambient O_2 (Horváth et al., 2012). Laskar et al. (2016) reconstructed the same $\Delta^{17}O$ signature for CO_2 from car exhausts measured in a tunnel.

The CO_2 released to the atmosphere by biomass burning is taken from the Global Fire Emissions Database version 4 (GFED4; Giglio et al., 2013). This data set is comprised by combining remotely sensed burned areas with modeled carbon pools from SiBCASA (van der Werf et al., 2010; van der Velde et al., 2014). The SiBCASA biomass burning emissions are available with a monthly time resolution and a spatial resolution of 1° × 1°. The isotopic signature of CO_2 released by biomass burning is determined by the isotopic signature of ambient O_2 and the wood intrinsic oxygen, resulting in an average signature of $\Delta^{17}O_{\mathrm{bb}} = -0.230‰$ for released CO_2 (Horváth et al., 2012).

2.4. Tropospheric Source of $\Delta^{17}O$ in CO_2

2.4.1. Tropospheric CO and $\Delta^{17}O$(CO) Budget

Most of the atmospheric CO_2 originates from the Earth surface, where it is released directly in the form of CO_2 through one of the processes as described in section 2.3. In addition, CO_2 can be produced in the atmosphere through oxidation of atmospheric CO by the hydroxyl radical OH,

$$\mathrm{CO} + \mathrm{OH} \rightarrow \mathrm{CO_2} + \mathrm{H}. \tag{21}$$

In this section we describe observed spatiotemporal patterns in $\Delta^{17}O(CO)$, the processes driving $\Delta^{17}O(CO)$ and the implications for the production of CO_2 isotopologues. Subsequently, we describe in section 2.4.2 how the production of CO_2 isotopologues from CO oxidation is implemented in our 3-D atmospheric transport model.

Measurements have revealed a large positive $\Delta^{17}O$ signature in atmospheric CO varying with season and location (measured at the per mil scale, similar to stratospheric CO_2 shown in Figure 2). Huff and Thiemens (1998) report that $\Delta^{17}O(CO)$ increases from a minimum of ~ 0.3‰ during winter to a maximum of ~ 2.7‰ during summer months in San Diego, California. Röckmann et al. (2002) measured a $\Delta^{17}O(CO)$ winter minimum of ~2‰ and summer maximum of ~8‰ at high northern latitude stations in Alert, Canada, and Spitsbergen, Norway. At the tropical station Izaña, Tenerife, the seasonal cycle of $\Delta^{17}O(CO)$ is much lower (~1‰) but the annual average value is rather similar at about 5‰ (Röckmann et al., 1998a).

The most important source of the large $\Delta^{17}O$ signature of CO is the oxidation of CO by OH (Röckmann et al., 1998a), which is not a mass-dependent process (the rate coefficients for oxidation of $C^{16}O$ and $C^{17}O$ are approximately equal, whereas the rate coefficient for $C^{18}O$ is substantially higher than for $C^{17}O$). This explains the observed seasonal cycle of $\Delta^{17}O(CO)$, since OH levels are higher during the summer months than during winter months, which is more pronounced at higher latitudes. Besides this main oxidation sink with a global magnitude of ~1 PgC/year (Holloway et al., 2000), CO is also taken up by soils at a global rate of 0.05–0.1 PgC/year (Sanhueza et al., 1998) which is a mass-dependent process and thus not affecting $\Delta^{17}O(CO)$.

Another contribution to the positive $\Delta^{17}O$ in CO is the ozonolysis of nonmethane hydrocarbons (Röckmann et al., 1998b), but its effect on the $\Delta^{17}O(CO)$ budget is less strong than the effect of the oxidation reaction. The main sources of CO (i.e., fossil fuel combustion, biomass burning and oxidation of atmospheric hydrocarbons) are considered to have a negligible contribution to the $\Delta^{17}O(CO)$ budget (Brenninkmeijer et al., 1999).

The sources and sinks of CO and their isotopic composition are uncertain and characterized by strong spatial and temporal variability but allow us to describe the following implications for the production of $\Delta^{17}O$ in CO_2. As the OH levels increase after winter, the mass-independent OH sink in equation (21) results in the production of CO_2 with a negative $\Delta^{17}O$ signature and the simultaneous increase in $\Delta^{17}O$ of the remaining CO. Due to the increasing enrichment of the substrate $C^{17}O$ and depletion of the substrate $C^{18}O$, the $\Delta^{17}O$ isoflux from CO to CO_2 will increase (i.e., become more positive or less negative) during the summer months. Since the sources of CO are largely mass dependent (i.e., with $\Delta^{17}O(CO)\approx 0$) and nearly all CO is removed through OH oxidation, we infer from mass conservation that the annual mean contribution of CO oxidation to the global budget of $\Delta^{17}O$ in CO_2 is minor (as will be confirmed in section 3.1.3.)

2.4.2. Production of CO_2 Isotopologues

To simulate the production of $\Delta^{17}O$ in CO_2 from CO oxidation, we use climatological fields for $C^{16}O$, $C^{17}O$ and $C^{18}O$ from Gromov (2013) with a global mean $\Delta^{17}O(CO)$ signature of 5.0‰ and climatological OH fields from Spivakovsky et al. (2000). The OH fields are available for each month on a native TM5 resolution of 1° × 1° horizontally and 60 vertical sigma-pressure levels. The climatological CO isotopologue fields are provided with a 5-day time resolution on a T42 spectral resolution and a vertical grid of 19 hybrid sigma-pressure levels and are regridded to match the temporal and spatial resolution of the OH fields.

We use a pressure-dependent relation for the rate of oxidation of CO from DeMore et al. (1997)

$$k_{CO+OH} = 1.5 \cdot 10^{-13} \cdot (1 + 0.6 \cdot p), \tag{22}$$

where p is the atmospheric pressure in the unit atmosphere and the unit of the rate coefficient k_{CO+OH} is cubic centimeter per molecule per second. In our model this rate coefficient is based on climatological pressure fields derived from the orography of the Earth surface. The rate coefficients for the oxidation of the isotopologues $C^{17}O$ and $C^{18}O$ are determined with respect to the overall rate coefficient from

$$\epsilon_n = k_{CO+OH}/k_{C^nO+OH} - 1, \tag{23}$$

for $n = 17$ or 18. The enrichment ϵ_n was measured in a controlled lab environment by Röckmann et al. (1998a) as $\epsilon_{17} = -0.21 \pm 1.30$‰ and $\epsilon_{18} = -9.29 \pm 1.52$‰ (for atmospheric pressure, according to Table 3.6 in Gromov, 2013). In a different lab study by Feilberg et al. (2002, 2005) enrichments of $\epsilon_{17} = 0 \pm 4$‰

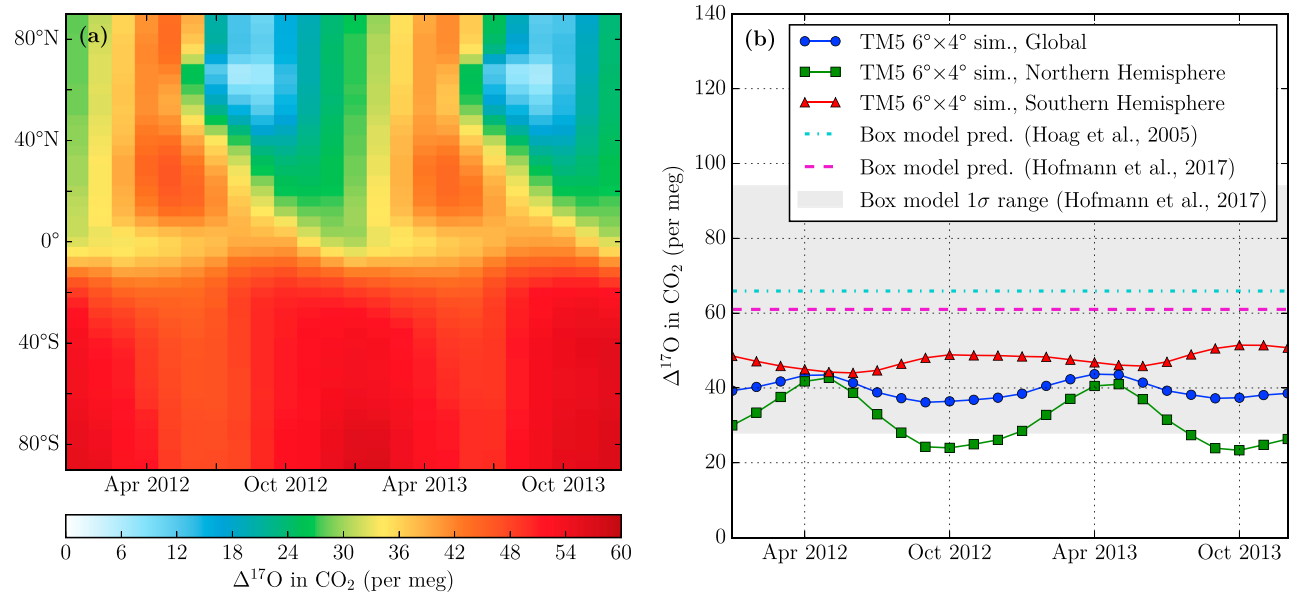

Figure 6. Monthly average of simulated $\Delta^{17}O$ in CO_2 for the lowest 500 m of the atmosphere using the TM5 model with base settings and a 6° × 4° horizontal resolution and 25 vertical levels. (a) Hovmöller diagram of $\Delta^{17}O$ in CO_2. (b) Time series of $\Delta^{17}O$ in CO_2 for TM5 integrated over NH, SH, and global domain, compared with predictions from box models by Hoag et al. (2005) and Hofmann et al. (2017).

and $\epsilon_{18} = -15 \pm 5‰$ were found. To test the consequences of applying the different rate coefficients, we have performed simulations for both lab results (simulations `CO_ROCK` and `CO_FEIL`, as summarized in Table 2).

The oxygen in atmospheric OH likely does not have an anomalous $\Delta^{17}O$ signature, since it equilibrates rapidly with atmospheric water vapor (Dubey et al., 1997; Lyons, 2001) and the $\Delta^{17}O$ signature of water vapor is negligible compared to that of CO (Uemura et al., 2010). To calculate the production of CO_2 isotopologues in our model, we assumed that $\Delta^{17}O(OH) = 0‰$, such that the temporal and spatial variation in the CO_2 production fields is determined fully by that of the CO isotopologues, the OH concentration, and the rate coefficients in equations (22) and (23). To prevent interference with the stratospheric model described in section 2.2, we only apply the chemical production of $\Delta^{17}O$ between the Earth surface and the 100-hPa level.

From the derived $C^{16}OO$, $C^{17}OO$, and $C^{18}OO$ production fields, we calculated the associated $\Delta^{17}O$ "flux" field. Subsequently, we scaled the $C^{18}OO$ fluxes such that the $\delta^{18}O$ fields for produced CO_2 equal our assumed fixed value of 41.5‰ (see section 2.1). Finally, we scaled the $C^{17}OO$ flux fields to reobtain the $\Delta^{17}O$ flux field . As mentioned in section 2.1, the motivation for using a fixed $\delta^{18}O$ for atmospheric CO_2 is that this considerably simplifies the coupling with the hydrological cycle. This method implies that the simulated $\Delta^{17}O$ signature is fully carried by the $C^{17}OO$ tracer in our atmospheric transport model.

Note that the contribution of mass-independent CO_2 through oxidation of atmospheric CO was not considered in the previous box models from Hoag et al. (2005) and Hofmann et al. (2017). Likewise, oxidation of CO is not included in our model runs with base settings (`BASE`), as summarized in Table 1. The resulting $\Delta^{17}O$ in atmospheric CO_2 for the simulations `CO_ROCK` and `CO_FEIL` (see Table 2) is presented and discussed in section 3.1.3.

3. Results

3.1. Global Model Simulations

3.1.1. $\Delta^{17}O$ in Tropospheric CO_2 for Base Model

In this section we show the results from the TM5 simulation with the base settings as summarized in Table 1 at a horizontal resolution of 6° × 4° and with 25 vertical levels. We started a simulation with an initial CO_2 distribution from data assimilation system CarbonTracker (Peters et al., 2007, 2010; van der Laan-Luijkx et al., 2017) and with $\Delta^{17}O = 0$ for each cell. After running the model for ~10 years, we obtained a steady state (no further increase in the mean annual $\Delta^{17}O$ signature) for the years 2012 and 2013 for which we show the results. We provide insight into the temporal and spatial patterns of modeled $\Delta^{17}O$ in CO_2 for the

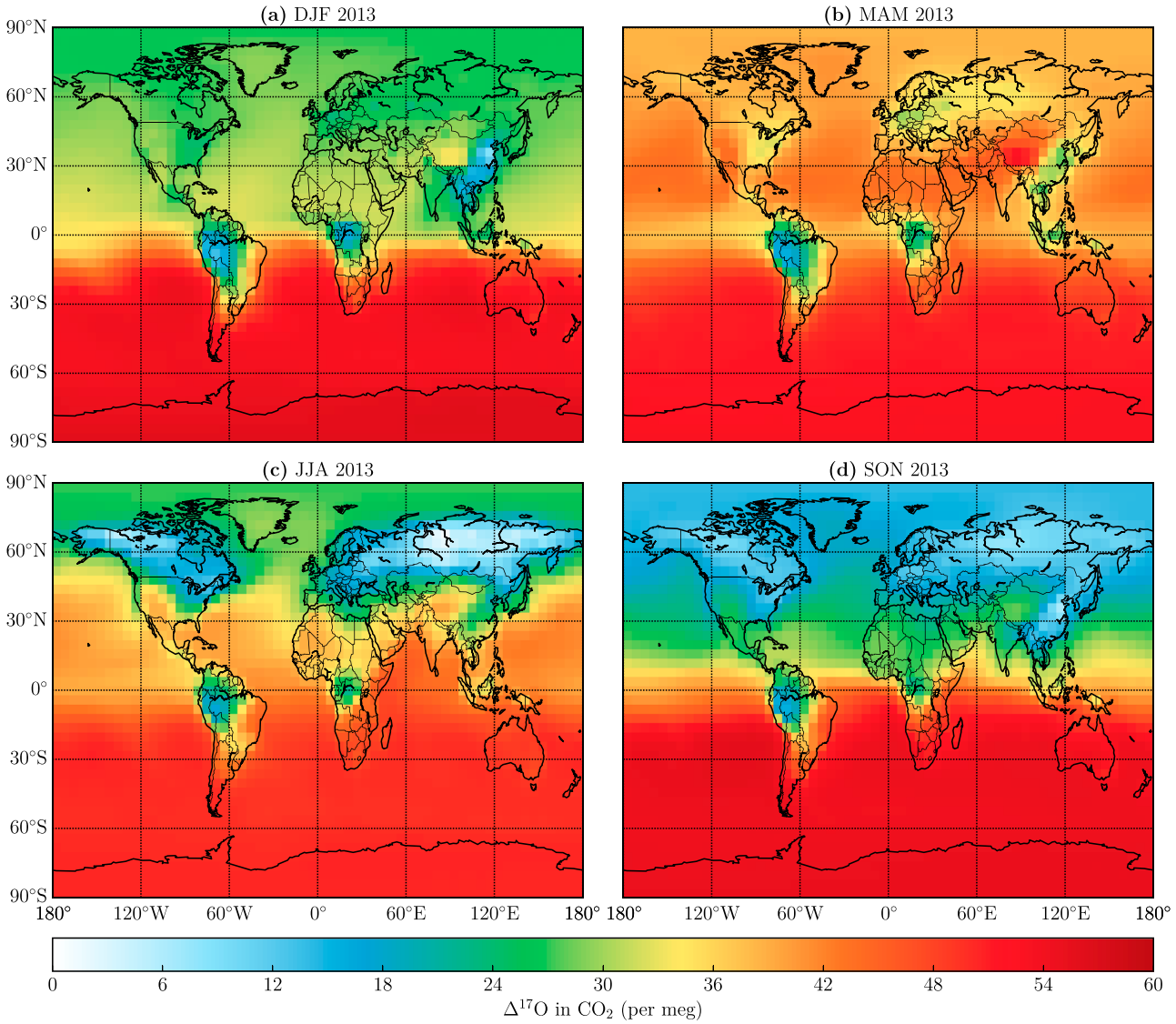

Figure 7. Seasonal average distributions of simulated $\Delta^{17}O$ in CO_2 for lowest 500 m of atmosphere from the TM5 model with base settings using a 6° × 4° horizontal resolution and 25 vertical levels. (a) Seasonal average for December, January, and February (DJF) 2013. (b) Seasonal average for March, April, and May (MAM) 2013. (c) Seasonal average for June, July, and August (JJA) 2013. (d) Seasonal average for September, October, and November (SON) 2013.

lowest ~500 m of the atmosphere (lowest four model levels). The CO_2 mass fluxes and corresponding $\Delta^{17}O$ isofluxes between the different reservoirs are discussed in section 3.1.2.

In Figure 6, we show the temporal variation of monthly average $\Delta^{17}O$ in CO_2. The Hovmöller diagram in Figure 6a shows that the Northern Hemisphere experiences the largest seasonal variation and that the decrease in $\Delta^{17}O$ occurs during the summer months for both hemispheres. Figure 6b shows the temporal variation of $\Delta^{17}O$ in CO_2 integrated over both hemispheres and for the global domain compared to box model predictions from Hoag et al. (2005) and Hofmann et al. (2017). Our 3-D model predicts an average $\Delta^{17}O$ signature of 39.6 per meg for CO_2 in the lowest 500 m of the atmosphere, which is roughly 20 per meg lower than the prediction from the box model by Hofmann et al. (2017). This is an expected result since the exchange of CO_2 with the biosphere, which represents the main sink of $\Delta^{17}O$, is higher in our model than for the box models. For the NH and SH we predict a mean $\Delta^{17}O$ signature of 31.6 and 47.6 per meg and a seasonal cycle with a peak-to-peak amplitude of 17.7 and 5.1 per meg, respectively. The spatial and temporal patterns in simulated $\Delta^{17}O$ confirm the potential of $\Delta^{17}O$ as a tracer of GPP.

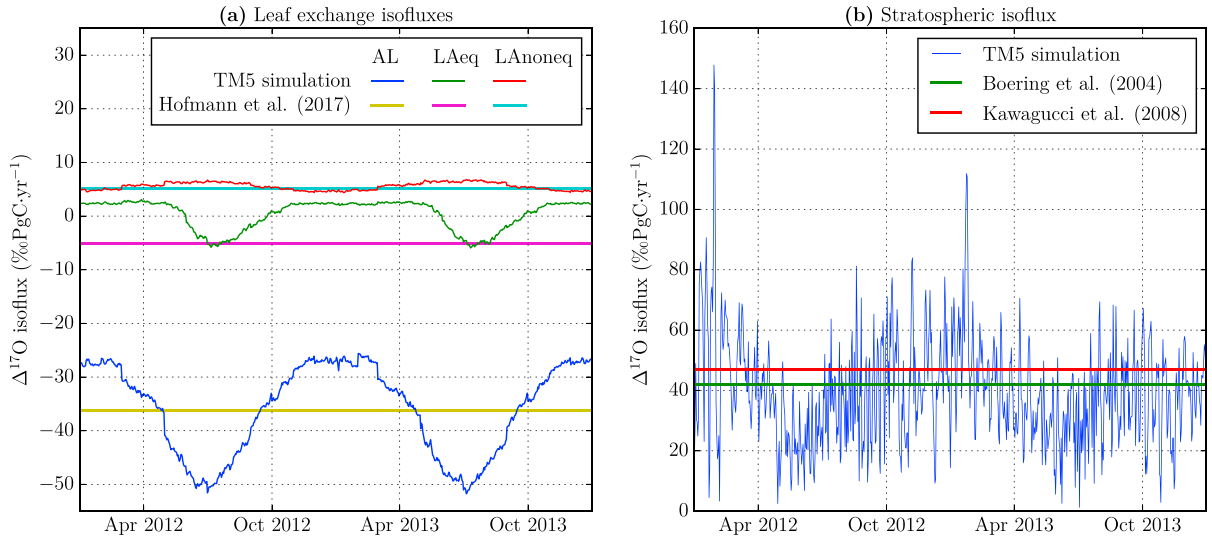

Figure 8. Daily time series of main $\Delta^{17}O$ isofluxes for TM5 simulation using base settings with 6° × 4° horizontal resolution and 25 vertical levels compared with independent global estimates. (a) Leaf exchange isofluxes from TM5 compared with predictions from the box model from Hofmann et al. (2017). (b) Net stratosphere-troposphere $\Delta^{17}O$ isoflux simulated with TM5 model compared with global estimates from Boering et al. (2004) and Kawagucci et al. (2008) based on observed N_2O–$\Delta^{17}O$ correlation and the stratospheric N_2O loss rate.

The spatial distribution of $\Delta^{17}O$ for the different seasons of 2013 is shown in Figure 7. Besides the North-South gradient that was already visible in Figure 6, we can see that the $\Delta^{17}O$ signature over oceans exceeds the $\Delta^{17}O$ above land, which can be explained by the strong effect of the biosphere on atmospheric $\Delta^{17}O$. In addition, the tropical regions in South America and Africa have low $\Delta^{17}O$ values during the entire year, with large zonal gradients, especially during December, January, and February and September, October, and November. Although the exchange of CO_2 between the biosphere and atmosphere is highest for the tropical regions, the lowest $\Delta^{17}O$ occurs in the NET. This is a direct consequence of the low $\Delta^{17}O$ signatures of soil water and leaf water (see Figure 5c) in the NET compared to the tropics. Note also that fossil fuel combustion can have a strong effect on the local $\Delta^{17}O$ signal, which explains the low $\Delta^{17}O$ in CO_2 simulated over parts of China.

3.1.2. CO_2 Mass Fluxes and $\Delta^{17}O$ Isofluxes for Base Model

To better understand the $\Delta^{17}O$ budget, we analyzed the magnitudes and spatiotemporal variations of the simulated CO_2 mass fluxes and $\Delta^{17}O$ isofluxes. The definition of the $\Delta^{17}O$ isoflux is

$$IF_{ij} = F_{ij} \cdot (\Delta^{17}O_i - \Delta^{17}O_{trop}), \tag{24}$$

where IF_{ij} and F_{ij} are, respectively, the $\Delta^{17}O$ isoflux and CO_2 mass flux from reservoir i to reservoir j. Furthermore, $\Delta^{17}O_{trop}$ and $\Delta^{17}O_i$ are the signatures for the troposphere and for the source reservoir (which can also be the troposphere, e.g., for the isoflux from the atmosphere to the ocean IF_{AO}). In this study we have used a reference level of $\Delta^{17}O_{trop} = 40$ per meg, which is representative for the lowest ~500 m of the atmosphere as described in section 3.1.1. The globally averaged yearly averaged CO_2 mass fluxes and $\Delta^{17}O$ isofluxes simulated by our TM5 model and the fluxes from the box models by Hofmann et al. (2017) and Hoag et al. (2005) are summarized in Table S2 of the supporting information.

In Figure 8 we show the global time series of the main biospheric and stratospheric $\Delta^{17}O$ isofluxes from the model simulation with base settings for the years 2012–2013. For the global biospheric $\Delta^{17}O$ isofluxes shown in Figure 8a, the atmosphere-leaf isoflux IF_{AL} has the largest seasonal variation with a peak-to-peak amplitude of ~25‰ PgC/year. IF_{AL} attains its peak (i.e., the most negative value) during the summer months in the Northern Hemisphere, similar to the seasonality in global carbon uptake by vegetation. The global equilibrated leaf-atmosphere isoflux IF_{LAeq} has a seasonal cycle with peak-to-peak amplitude of ~10‰ PgC/year and is changing sign during the course of the year. The sign change in IF_{LAeq} is related to the change in the isotopic signature of leaf water (see section 2.3.1) and the selected reference level $\Delta^{17}O_{trop}$. Finally, we see that global mean nonequilibrated leaf-atmosphere isoflux $IF_{LAnoneq}$ is nearly constant during the year. Note

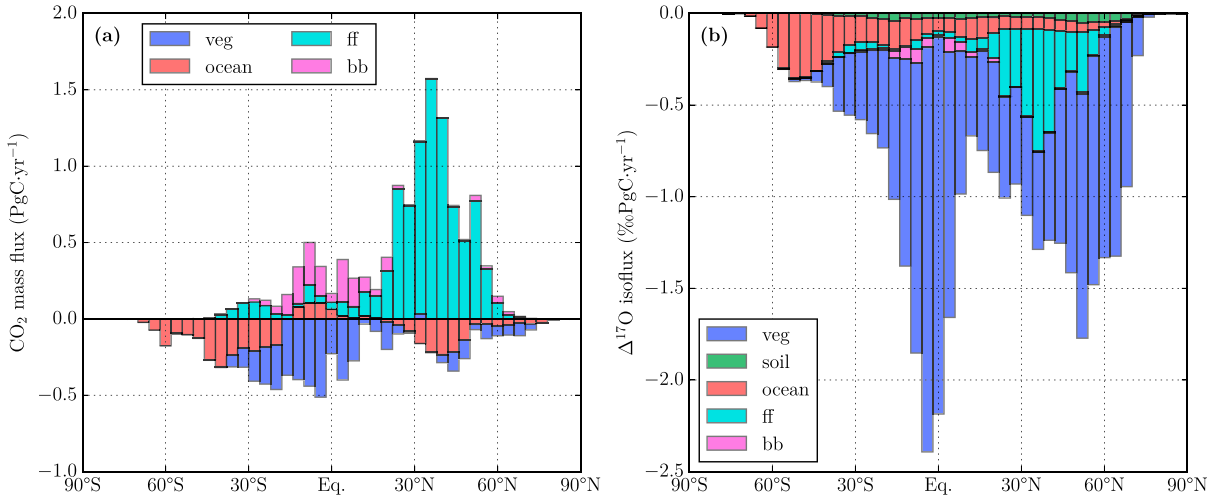

Figure 9. Net CO_2 mass fluxes (a) and net $\Delta^{17}O$ isofluxes (b) as function of latitude resulting from vegetation exchange ("veg"), soil invasion, ocean exchange, fossil fuel combustion ("ff"), and biomass burning ("bb") for TM5 simulation with base settings, 6° × 4° horizontal resolution, and 25 vertical levels.

that for all biospheric fluxes shown in Figure 8a the average value (and hence also the occurrence of sign changes for IF_{LAeq}) is sensitive to the reference level $\Delta^{17}O_{trop}$.

The global net stratospheric $\Delta^{17}O$ isoflux in Figure 8b has a mean value of ∼40‰ PgC/year, which agrees well with the estimates from Boering et al. (2004) and Kawagucci et al. (2008) that were derived from the observed N_2O–$\Delta^{17}O$ correlation and the estimated stratospheric N_2O loss rate. Also, our global mean $\Delta^{17}O$ stratospheric isoflux is close to the simulated flux by Liang et al. (2008). Our simulated stratospheric $\Delta^{17}O$ isoflux has a seasonal cycle with a peak-to-peak amplitude of ∼40‰ PgC/year. On top of this, a relatively large day-to-day variability is associated with the stratospheric $\Delta^{17}O$ isoflux. The average value of the stratospheric isoflux is not sensitive (compared to biospheric isofluxes) to small changes in the reference level, since $\Delta^{17}O_{strat} \gg \Delta^{17}O_{trop}$ whereas $\Delta^{17}O_{leaf} \approx \Delta^{17}O_{trop}$. During the Northern Hemispheric winter months, the global stratospheric influx of $\Delta^{17}O$ is relatively high, while at the same time the biospheric sink of $\Delta^{17}O$ is relatively weak, resulting in an increase of $\Delta^{17}O$ in atmospheric CO_2 on the global scale (which is visible in Figure 6). An overview of the temporal variation of all global CO_2 mass fluxes and $\Delta^{17}O$ isofluxes during the years 2012–2013 is given in Figures S2 and S3 of the supporting information.

The latitudinal distribution of the annual mean net CO_2 mass fluxes and $\Delta^{17}O$ isofluxes for 2012–2013 is shown in Figure 9 for different surface processes. Figure 9a clearly shows the dominance of fossil fuel combustion ("ff") in the CO_2 budget. In the warm tropics, the ocean is a source of CO_2 to the atmosphere ($F_{OA} > F_{AO}$), whereas the ocean is a net sink of CO_2 in the extratropics. Across all latitudes, vegetation exchange and biomass burning act as a net sink and source, respectively, and both processes peak in the tropical region. Soil invasion has no net contribution to the CO_2 budget, since we assume that the uptake is equal to the release for each grid cell. The $\Delta^{17}O$ isofluxes in Figure 9b are negative for all latitudinal bands for each surface process. The $\Delta^{17}O$ isofluxes are dominated by the vegetation fluxes, although the contribution of fossil fuel combustion is significant in the Northern Hemisphere. Soil invasion $\Delta^{17}O$ isofluxes are relatively small, for this simulation with base settings. More details for the contribution of different processes (e.g., the ingoing and outgoing leaf fluxes) as a function of latitude are presented in Figures S4 and S5 of the supporting information.

3.1.3. Model Sensitivity Analysis

Here we discuss the results of a sensitivity analysis for $\Delta^{17}O$ in CO_2. We have changed input values for the stratospheric N_2O–$\Delta^{17}O$ fit coefficients, the soil water and leaf water $\Delta^{17}O$ signatures, the soil invasion fluxes, and the oxidation of atmospheric CO, as summarized in Table 2. In Table 3 we report the mean value and the peak-to-peak amplitude for $\Delta^{17}O$ in CO_2 for the lowest 500 m of the atmosphere for a selection of simulations with modified input settings. The peak-to-peak amplitude of global $\Delta^{17}O$ was determined by fitting a sine function on the monthly values for global $\Delta^{17}O$ for the years 2012 and 2013.

Table 3
Overview of the Mean Value and the Peak-to-Peak Amplitude of the Seasonal Cycle of $\Delta^{17}O$ in CO_2 for the Lowest 500 m of the Atmosphere for Different TM5 Model Simulations with Horizontal Resolution of 6° × 4° and with 25 Vertical Levels

	Mean $\Delta^{17}O$ value (first column; per meg) Peak-to-peak $\Delta^{17}O$ amplitude (second column, enclosed in parentheses; per meg)						
Simulation	Global	NH	SH	Zotino	Mauna Loa	Manaus	South Pole
BASE	39.6 (6.5)	31.6 (17.7)	47.6 (5.1)	19.0 (36.1)	36.2 (19.5)	23.2 (2.9)	52.5 (7.4)
ST_LOWER	19.6 (5.4)	12.6 (14.4)	26.6 (3.9)	1.5 (31.4)	16.3 (15.5)	8.2 (2.9)	30.4 (5.5)
ST_UPPER	59.6 (7.7)	50.6 (21.1)	68.7 (6.3)	36.4 (40.9)	56.1 (23.5)	38.1 (2.9)	74.5 (9.2)
SOIL_CONST	40.5 (4.7)	34.7 (14.3)	46.3 (5.3)	27.8 (23.9)	38.7 (16.8)	18.5 (1.3)	51.1 (7.5)
LEAF_CONST	34.5 (6.7)	26.2 (17.8)	42.8 (4.9)	13.8 (36.1)	30.8 (19.7)	20.0 (2.3)	47.7 (7.1)
RESP_240	32.1 (6.4)	23.5 (17.4)	40.8 (4.9)	9.1 (35.3)	28.3 (19.2)	17.6 (3.0)	45.7 (7.2)
RESP_450	27.6 (6.3)	18.5 (17.1)	36.7 (4.8)	2.7 (34.5)	23.5 (18.9)	14.8 (3.0)	41.7 (7.0)
HYD_240	30.4 (6.6)	21.9 (17.7)	39.0 (4.9)	9.5 (35.6)	26.6 (19.3)	16.4 (3.1)	43.9 (7.1)
HYD_450	25.5 (6.6)	16.6 (17.5)	34.3 (4.7)	4.0 (35.5)	21.4 (19.0)	13.0 (3.1)	39.2 (6.9)
CO_ROCK	40.0 (6.5)	32.0 (17.6)	48.0 (5.1)	19.4 (36.0)	36.6 (19.4)	23.5 (2.9)	52.8 (7.4)
CO_FEIL	37.7 (6.4)	29.8 (17.5)	45.6 (5.1)	17.4 (35.5)	34.2 (19.3)	21.6 (3.1)	50.4 (7.3)

Note. The input settings for each simulation are summarized in Table 2. The global and hemispheric results are discussed in section 3.1.3, and the results for Zotino (60.80°N, 89.35°E), Mauna Loa (19.54°N, 155.58°W), Manaus (2.15°S, 59.00°W), and South Pole (90°S) are discussed in section 3.2.2. NH = Northern Hemisphere; SH = Southern Hemisphere.

According to Table 3, the change in the stratospheric N_2O–$\Delta^{17}O$ fit coefficients results in a change of roughly +20 and −20 per meg for the 95% upper (ST_UPPER) and lower limit (ST_LOWER) fits, respectively (see Figure 2b for the slope and offset of the fits) relative to the base model run (BASE). Clearly, the selected stratospheric fit is a key parameter for the resulting $\Delta^{17}O$ in tropospheric CO_2. Also, we see that the SH-NH difference and the amplitude of global $\Delta^{17}O$ increases when using the 95% upper limit confidence interval fit. As expected, the changes in these characteristics of the $\Delta^{17}O$ distribution are reversed when using the 95% lower limit confidence interval fit. On annual basis, the effect of changing the stratospheric fit coefficients is smallest for the tropical forests in the Amazon and in Central Africa, as shown in Figure S6 of the supporting information, which is caused by the rapid exchange between the atmosphere and biosphere in these regions.

In the base model run, we use a spatial distribution for the soil water signature $\Delta^{17}O_{soil}$ and spatial and temporal variation in the leaf water signature $\Delta^{17}O_{leaf}$ based on the local relative humidity, according to equations (15) and (16). We performed TM5 simulations with a constant soil water signature $\Delta^{17}O_{soil} = -5$ per meg (SOIL_CONST) and with a constant transpiration exponent $\lambda_{transp} = 0.5156$ (LEAF_CONST; values that are also used in the box model from Hofmann et al., 2017). It should be noted that in this analysis we are changing not only the time and/or space dependency of $\Delta^{17}O_{soil}$ and $\Delta^{17}O_{leaf}$ but also their global average value. In the base model run the global mean values are $\Delta^{17}O_{soil} = -10.2$ per meg and $\lambda_{transp} = 0.5160$. Table 3 shows that changing to a constant $\Delta^{17}O_{soil} = -5$ per meg has a small effect on global mean $\Delta^{17}O$ in atmospheric CO_2, whereas using a constant $\lambda_{transp} = 0.5160$ results in a decrease of 5.1 per meg in global mean $\Delta^{17}O$. Finally, we see that changing the soil water signature to $\Delta^{17}O_{soil} = -5$ per meg leads to decreases in both the North-South difference and the amplitude of global $\Delta^{17}O$. In Figure S7 of the supporting information we show the annual mean difference of $\Delta^{17}O$ for the TM5 simulations with modifications in the water signatures relative to the base model run.

The effect of a change in the global magnitude and the spatial distribution of the soil invasion flux can also be seen in Table 3. An increase from the base value of 30 to 240 PgC/year or even 450 PgC/year leads to a decrease in the global mean $\Delta^{17}O$ signature of atmospheric CO_2, where the magnitude of the $\Delta^{17}O$ drop also depends on the spatial distribution of the soil invasion flux. For respiration scaling (BASE, RESP_240, and RESP_450) the soil invasion fluxes are mostly present in the tropical region, whereas for hydrogen scaling (HYD_240 and HYD_450) the soil invasion fluxes extend to higher latitudes, which have a lower $\Delta^{17}O_{soil}$ signature and hence result in a lower $\Delta^{17}O$ for atmospheric CO_2. Also, we see in Table 3 that increasing the soil invasion fluxes leads to a small decrease in the amplitude of global and hemispheric $\Delta^{17}O$. In Figure S8

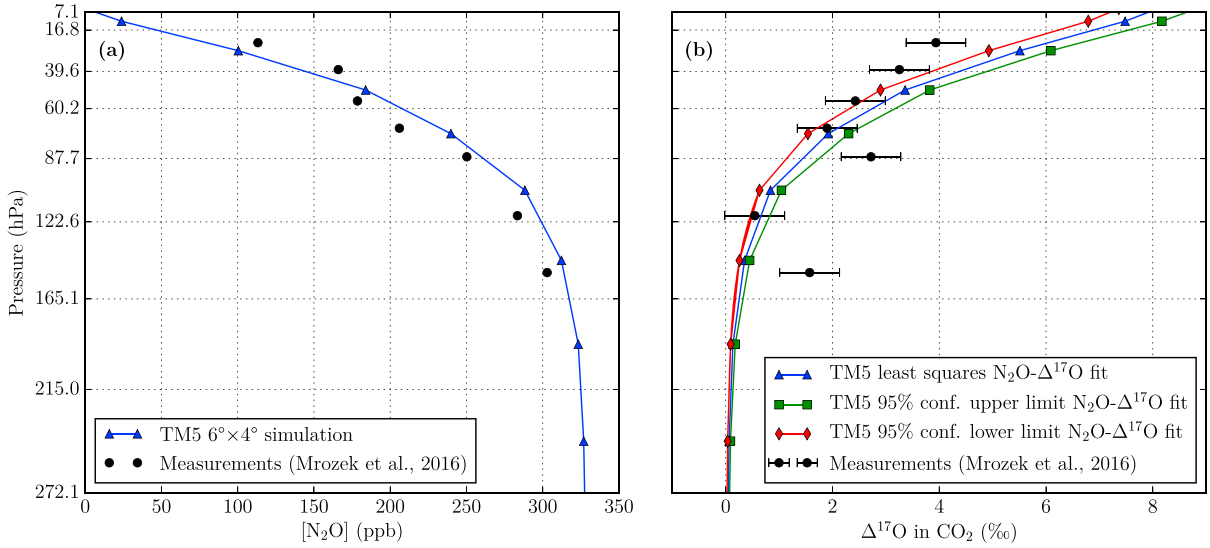

Figure 10. Comparison of vertical profiles measured over Sodankylä (67.35°N, 26.93°E; Mrozek et al., 2016) with TM5 model simulations with horizontal resolution of 6° × 4° and with 25 vertical levels. The ticks on the vertical axis coincide with the cell boundaries in the TM5 model with 25 vertical levels. (a) Stratospheric profile of N_2O mole fraction. (b) Stratospheric profile of $\Delta^{17}O$ in CO_2 compared with TM5 least squares N_2O–$\Delta^{17}O$ fit simulation (`BASE`), 95% confidence upper limit fit simulation (`ST_UPPER`) and 95% confidence lower limit fit simulation (`ST_LOWER`).

of the supporting information we show the global mean $\Delta^{17}O$ distribution for changes in the soil invasion fluxes.

Finally, we show in Table 3 that incorporating the CO + OH reaction with the enrichment ϵ_{CO+OH} from Röckmann et al. (1998a) (`CO_ROCK`) has a small positive effect on the resulting $\Delta^{17}O$ of atmospheric CO_2, whereas a larger negative effect was found for the fractionation factors from Feilberg et al. (2005) (`CO_FEIL`). Based on the enrichment coefficients given in section 2.4.2, we expect that more ^{18}O-enriched CO_2 is produced in `CO_FEIL` than for `CO_ROCK`, which explains its lower resulting $\Delta^{17}O$ signature in atmospheric CO_2. Because the coefficients from Röckmann et al. (1998a) were also used to produce the CO isotopologue fields by Gromov (2013), we consider the results for `CO_ROCK` to be most representative. In Figure S9 of the supporting information we show the distribution of the annual mean anomalies for the calculated $\Delta^{17}O$ relative to the base model run.

3.2. Local Model Simulations

3.2.1. Model-Measurement Comparisons

To test the ability of our model to simulate $\Delta^{17}O$ in atmospheric CO_2, we compare our model results with a stratospheric profile measured above Sodankylä, Finland (Mrozek et al., 2016) and with tropospheric measurement series for Göttingen, Germany (Hofmann et al., 2017) and Taipei, Taiwan (Liang et al., 2017b). We selected these two data sets, because the measurement periods overlap (partially) with our model output for years 2010–2014. It should be noted that we are using a relatively coarse resolution for our model (a 6° × 4° horizontal resolution and 25 vertical levels) and that the model output are daily averages and therefore not fully representative for the observations.

In Figure 10, our TM5 model results are shown alongside the N_2O mole fraction and $\Delta^{17}O$ in CO_2 profiles that were obtained from an AirCore with Stratospheric Air Sub-sampler by Mrozek et al. (2016) above Sodankylä, Finland (67.35°N, 26.93°E) on 5 November 2014. Note that the N_2O mole fractions that are reported by Mrozek et al. (2016) are not directly measured but inferred from measurements of CH_4. The profile of N_2O mole fractions from our simulation agrees reasonably well with the "measured" N_2O profile. Contrary to the measured $\Delta^{17}O$ in CO_2 signatures, the simulated profile shows a monotonic increase with altitude. For the two observations at highest altitudes (at 24 and 39 hPa) we find that the simulated N_2O is too low and that the simulated $\Delta^{17}O$ in CO_2 is too high, which suggests that the sampled air is younger than simulated in the transport model for these altitudes. The opposite is found for two of the three lowest observations (at 87 and 151 hPa) indicating that the sampled air was older than the simulated air. Note

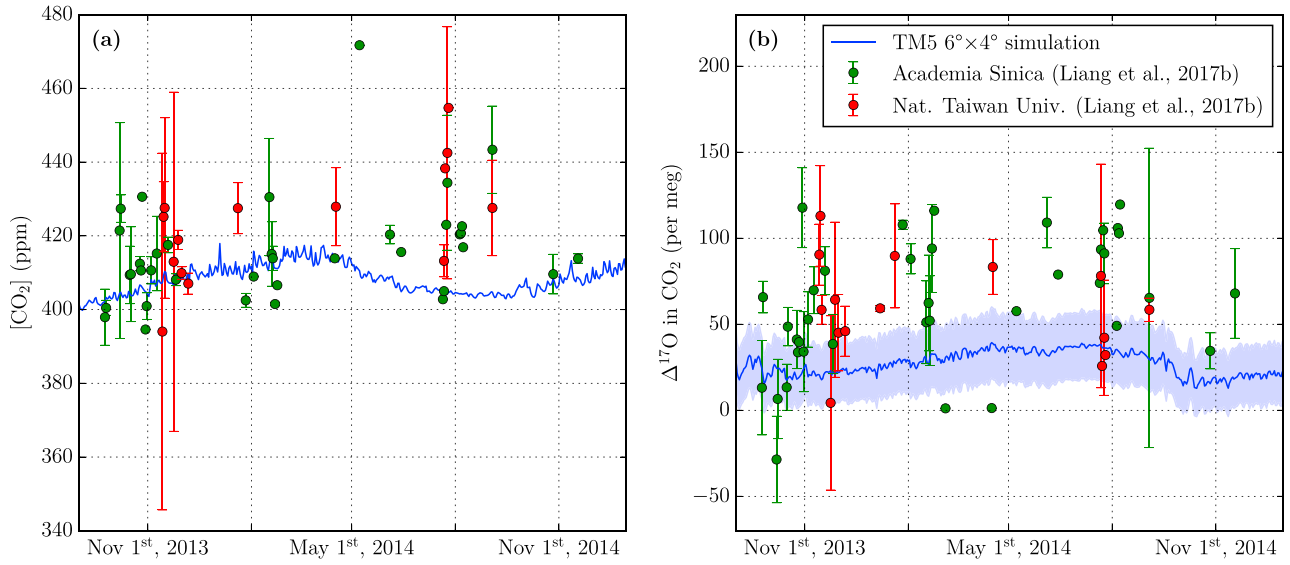

Figure 11. Comparison of tropospheric measurements for the Academia Sinica campus (25.04°N, 121.61°E) and the National Taiwan University (25.01°N, 121.54°E) in Taipei, Taiwan, from Liang et al. (2017b) with daily model predictions for the lowest 35 m from TM5 with horizontal resolution of 6° × 4° and 25 vertical levels. (a) CO_2 mixing ratios. (b) $\Delta^{17}O$ in CO_2. The shading indicates the spread in model estimates for the 95% confidence interval for the N_2O–$\Delta^{17}O$ fit for stratospheric CO_2 (obtained from simulations `ST_LOWER` and `ST_UPPER`).

that the comparison of our model results with the data from Mrozek et al. (2016) is independent, since the experimental data from Mrozek et al. (2016) were not used as input for the N_2O–$\Delta^{17}O$ fit.

In Hofmann et al. (2017), model predictions from an early version of our model (see section S2 of the supporting information for an overview of the differences with our current model) were compared with measurements of $\Delta^{17}O$ in CO_2 for Göttingen (51.56°N, 9.95°E) and Mt. Brocken (51.80°N, 10.62°E). We have repeated the analysis with our updated model and again find that there is a seasonal cycle in $\Delta^{17}O$ that is driven by the biosphere. Also, we again find that our model does not show the significant drop in $\Delta^{17}O$ that is reported based on observations (respectively a mean $\Delta^{17}O$ of −12.8 and −108.2 per meg before and after 1 July 2011). This unexplained, large drop in the reported observations is discussed in more detail in section 6.2 of Hofmann et al. (2017). A comparison of the measured CO_2 mole fraction and its $\Delta^{17}O$ signature for Göttingen (51.56°N, 9.95°E) and Mt. Brocken (51.80°N, 10.62°E) with model predictions for the lowest level in TM5 (lowest ∼35 m) is given in Figure S10 of the supporting information.

We also compare our model predictions for $\Delta^{17}O$ in tropospheric CO_2 with measurement data obtained at the Academia Sinica campus (25.04°N, 121.61°E) and the National Taiwan University (25.01°N, 121.54°E) in Taipei, Taiwan, from Liang et al. (2017b). In Figure 11 we compare the measured and simulated CO_2 mole fractions and the $\Delta^{17}O$ signature. The uncertainty bar that is associated with the measured CO_2 mole fractions is determined from the deviation between measurements taken at different times on the same day, showing the importance of local contributions and the development of the atmospheric boundary layer. The shading in Figure 11b indicates the spread related to the 95% confidence interval for the N_2O–$\Delta^{17}O(CO_2)$ coefficients (slope and offset) that is used in the stratospheric module. The spread in model predictions for the different representations of the stratospheric source is substantial (∼40 per meg range) but cannot fully explain the model-measurement discrepancy for this location. Compared to Göttingen, there is a smaller contribution of the biospheric fluxes since Taipei is surrounded by ocean. In addition, we expect a lower seasonality of the biosphere at the latitude of Taipei compared to Göttingen. Contrary to measurement series from Göttingen, our model predictions are lower (mean value of 31.1 per meg) than the $\Delta^{17}O$ measurements from Taipei (mean value of 58.7 per meg).

3.2.2. Future Measurements

The currently available measurement series for $\Delta^{17}O$ of tropospheric CO_2 have in common that the air was collected in the vicinity of the research groups that performed the measurements. Our objective here is to make use of our 3-D model predictions to identify locations for which measurements of $\Delta^{17}O$ in CO_2 would be valuable for a better understanding of the global budget of $\Delta^{17}O$ in CO_2 and further model development.

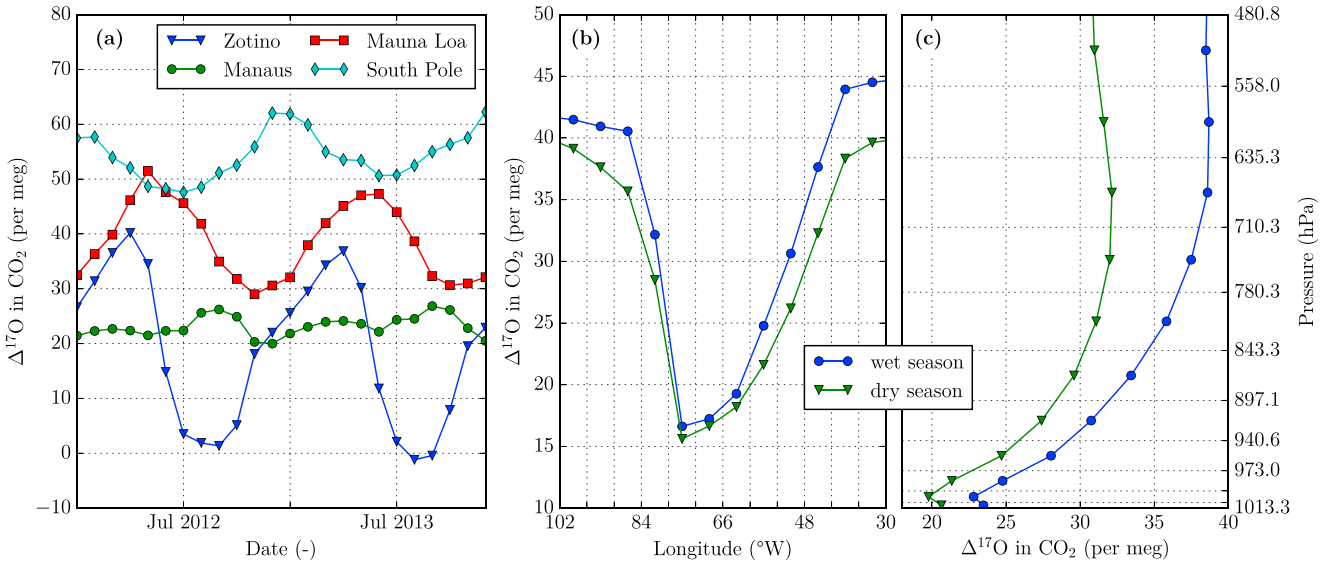

Figure 12. TM5 model predictions for $\Delta^{17}O$ in atmospheric CO_2 using base model settings with a horizontal resolution of 6° × 4° and with 25 vertical levels for selected locations. (a) Time series of $\Delta^{17}O$ in CO_2 for the lowest 500 m of the atmosphere for Zotino (60.80°N, 89.35°E), Mauna Loa (19.54°N, 155.58°W), Manaus (2.15°S, 59.00°W), and South Pole (90°S). (b) Longitudinal cross section through Manaus of $\Delta^{17}O$ in CO_2 for the lowest 500 m of the atmosphere in the dry season (defined here as months in the range July to October) and wet season; the vertical grid lines correspond to the longitudinal boundaries of the TM5 grid. (c) Vertical profile over Manaus of $\Delta^{17}O$ in CO_2 in the dry and wet seasons; the horizontal grid lines correspond to the vertical TM5 hybrid sigma-pressure levels.

A global map of the peak-to-peak amplitude of simulated $\Delta^{17}O$ in CO_2 is shown in Figure S11a of the supporting information. We have selected four locations for which we describe the simulated patterns of $\Delta^{17}O$ in CO_2 in more detail.

Figure 12a shows the $\Delta^{17}O$ signature for CO_2 in the lowest 500 m of the atmosphere for a selection of locations. Zotino (60.80°N, 89.35°E) is the location of the Zotino Tall Tower Observatory (Heimann et al., 2014), where we expect a seasonal cycle of 36.1 per meg (see also Table 3), which is substantially larger than the measurement uncertainty of currently available measurement techniques (see also section 1). Also, the mean value of $\Delta^{17}O$ at Zotino can be used to better constrain the magnitude of soil invasion fluxes (see Table 3). This site was also used in a study of the $\delta^{18}O$ in CO_2 signal by Cuntz et al. (2002).

Mauna Loa (19.54°N, 155.58°W) and South Pole (90°S) are background stations that are famous for their long-standing CO_2 records that are operated by the National Oceanic and Atmospheric Administration and the Scripps Institution of Oceanography. The time series of $\Delta^{17}O$ for CO_2 in the lowest 500 m of the atmosphere (above the local surface) for Mauna Loa and South Pole in Figure 12a exhibit a seasonal cycle in antiphase with each other. Also, South Pole is an interesting location because we expect a high annual mean $\Delta^{17}O$ signature. Dry air samples from the South Pole (British Antarctic Survey station) were collected in 2017 and are currently being analyzed for their $\Delta^{17}O$ in CO_2 signatures by the Centre for Isotope Research in Groningen, the Netherlands.

Also, we included model predictions of $\Delta^{17}O$ in CO_2 for Manaus (2.15°S, 59.00°W), the location of the Amazon Tall Tower Observatory (Andreae et al., 2015). Although the annual variation of $\Delta^{17}O$ in CO_2 is small in the lowest 500 m of the atmosphere for Manaus, there is a relatively strong gradient for $\Delta^{17}O$ in the longitudinal direction across Manaus (Figure 12b) and a strong vertical gradient above Manaus (Figure 12c). Measurements in and around the Amazon region that are ongoing since February 2018 and analyzed at the LaGEE lab in Brazil could show whether these predicted features in the $\Delta^{17}O$ distribution can be observed. The zonal mean annual mean vertical profile for $\Delta^{17}O$ in CO_2 as a function of latitude can be seen in Figure S11b of the supporting information.

4. Discussion

4.1. Possible Improvements of Model for $\Delta^{17}O$ in CO_2

In this section we discuss some model features that could be added to or improved with respect to our current 3-D model for $\Delta^{17}O$ in CO_2. In our current model we represent the stratospheric source of $\Delta^{17}O$ by simulating N_2O and converting stratospheric N_2O mole fractions into $\Delta^{17}O$ signatures based on their observed correlation as described in section 2.2.1. Although we feel that this is a robust and straightforward approach, we generally prefer to simulate the actual physical processes. As more details of the production process are unfolded by the scientific community, we foresee that it becomes more feasible to implement an explicit description of the production of $\Delta^{17}O$ in CO_2 in future model versions.

To calculate the atmosphere leaf fluxes F_{AL} and F_{LA}, we use GPP from SiBCASA at a 3-hourly temporal resolution and GPP-weighted c_i/c_a values from SiBCASA at a monthly temporal resolution as described in section 2.3.1. Also, we assume in our current model that leaf respiration is a constant fraction of 12% of GPP, similar to Ciais et al. (1997a). In future studies we intend to use c_i/c_a values and leaf respiration from SiBCASA at a 3-hourly temporal resolution to be fully consistent with the temporal resolution of GPP. In the comprehensive $\delta^{18}O$ model from Cuntz et al. (2003a, 2003b) these components are also simulated at the same temporal resolution.

For some input fields we use year-specific data, such as the meteorological data ERA-Interim (Dee et al., 2011) that drives the atmospheric transport in TM5. Also, the vegetation-atmosphere fluxes from the SiB-CASA model are calculated using the ERA-Interim meteorology. For other input fields, we resort to annually repeating fields, such as for the CO isotopologue fields (Gromov, 2013) and the OH fields (Spivakovsky et al., 2000). In general, we preferably use year-specific input data to capture interannual variability of the different processes. Especially for CO oxidation, we expect some interannual variability due to the irregular occurrence of wildfires (which is major source of CO; Holloway et al., 2000) that we are now not able to simulate.

Another possible improvement is the resolution of the transport model for the performed simulations, which is relatively coarse (a horizontal resolution of $6° \times 4°$ and a vertical resolution of 25 layers). A finer horizontal resolution could lead to better agreement with local surface measurements, and a finer vertical resolution could be more representative for the STE, which is of importance to the $\Delta^{17}O$ in CO_2 budget and its ability to be used as tracer of GPP, as discussed in section 4.3. For follow-up studies focusing on specific regions, we intend to use finer spatial resolutions.

Finally, a valuable extension of this model would be to implement a "tracer tagging" method that allows to disentangle the contributions of different processes (e.g., biosphere exchange or fossil fuel combustion) on the resulting $\Delta^{17}O$ signature of CO_2. This would allow to effectively attribute the seasonal patters, interannual variability, or local disturbances that appear in the simulated $\Delta^{17}O$ signature to these processes. Such a tracer tagging technique was also used in the $\delta^{18}O$ studies from Ciais et al. (1997a, 1997b), Peylin et al. (1997, 1999), and Cuntz et al. (2003a, 2003b) to quantify the contribution of different processes to the simulated $\delta^{18}O$ signature for atmospheric CO_2.

4.2. Required Measurements of $\Delta^{17}O$ in CO_2

In this section we discuss issues related to the measurements of $\Delta^{17}O$ in CO_2. For $\delta^{18}O$ in CO_2 there is a vast network of well characterized measurement stations operated by the National Oceanic and Atmospheric Administration (NOAA) and collaborating organizations that measure $\delta^{18}O$ in CO_2 at a regular basis in addition to other atmospheric compounds and meteorological variables. These flasks are typically already collected with dried air, and with new measurement techniques for $\Delta^{17}O$ in CO_2 the air in these flasks is sufficient for a high-precision ($\pm$ 20 per meg) analysis. The opportunity to start a global characterization of actual signatures followed by a monitoring effort across a subset of most interesting sites thus could be seized. In section 3.2.2, we describe in more detail four locations where measurements have, or could be, started using existing resources.

Besides these observations of $\Delta^{17}O$ on the global scale that can help to understand the budget of $\Delta^{17}O$ in CO_2, there is also a need to measure the individual processes that affect $\Delta^{17}O$ in CO_2. The value of experiments that unravel the remaining uncertainties about the stratospheric production of $\Delta^{17}O$ was already mentioned in section 4.1. Also, controlled laboratory measurements on the effect of plant assimilation on the $\Delta^{17}O$ signature of atmospheric CO_2 could be valuable to test the assumptions used in our current model that are

for a large part based on earlier works on $\delta^{18}O$ in CO_2 (e.g., Gillon & Yakir, 2000, 2001). Furthermore, field scale studies can help to quantify the effect of these leaf-scale processes and entrainment on $\Delta^{17}O$ in the atmospheric boundary layer (as done for $\delta^{13}C$ and $\delta^{18}O$ by Vilà-Guerau de Arellano et al., 2019)

4.3. Potential of $\Delta^{17}O$ in CO_2 as Tracer of GPP

In this final discussion section we reflect on the potential of $\Delta^{17}O$ in CO_2 to function as a tracer of GPP. One of the main requirements for its use as tracer of GPP is that the stratospheric influx of $\Delta^{17}O$ in CO_2 can be quantified accurately. However, as described in section 2.2.3, estimates for the STE vary considerably. Combination with other tracers (e.g., ^7Be, as described by Dutkiewicz & Husain, 1985) might be necessary to reduce the uncertainty in STE.

One of the key variables in the budget of $\Delta^{17}O$ in CO_2 is the c_i/c_a ratio that relates the gross exchange fluxes between atmosphere and leaf to GPP as described in section 2.3.1. Cuntz (2011) pointed out in a commentary about the GPP estimate by Welp et al. (2011) that uncertainty in the c_i/c_a ratio (or the percentage of the CO_2 that diffuses into a leaf that is fixed) can have significant effects on the inferred GPP. This exemplifies the necessity to better constrain c_i/c_a, which might be achieved with $\delta^{13}C$ observations (Peters et al., 2018).

Similarly, the large uncertainty in the magnitude of soil invasion fluxes that was reported by Wingate et al. (2009) has implications for the potential use of $\Delta^{17}O$ in CO_2 as a tracer of GPP. If the soil invasion fluxes are underestimated, this could lead to overestimating GPP since these processes have a similar effect on $\Delta^{17}O$ in CO_2. The ongoing research on carbonic anhydrase in soils from the COS community might also lead to better quantification of the CO_2 soil invasion fluxes and as such benefit the use of $\Delta^{17}O$ in CO_2 as tracer of GPP.

Finally, we address the effect of the hydrological cycle on the budget of $\Delta^{17}O$ in atmospheric CO_2. The main reason to explore the use of $\Delta^{17}O$ as tracer for GPP instead of $\delta^{18}O$ was that $\Delta^{17}O$ is hardly sensitive to the hydrological cycle which greatly simplifies its interpretation and modeling according to Hoag et al. (2005). Still, we have put much effort in calculating the $\Delta^{17}O$ isotopic composition of different water reservoirs (e.g., soil water and leaf water, as discussed in section 2.3.1) and we find that changing these values can have a significant effect at high northern latitudes, as described in section 3.1.3. Also, a recent study by Tian et al. (2018) shows that $\Delta^{17}O$ of precipitation collected at Indianapolis (Indiana, USA), can vary considerably within months. As such, the use of $\Delta^{17}O$ in CO_2 could be more involved than originally envisioned by Hoag et al. (2005) depending on the specifics of the application.

5. Conclusions

We developed a 3-D model framework for $\Delta^{17}O$ (defined as $\Delta^{17}O = \ln(\delta^{17}O + 1) - \lambda_{RL} \cdot \ln(\delta^{18}O + 1)$, with $\lambda_{RL} = 0.5229$) in atmospheric CO_2, using the terrestrial biosphere model SiBCASA and atmospheric transport model TM5. In our model framework, the stratospheric source of $\Delta^{17}O$ in CO_2 is based on the observed N_2O–$\Delta^{17}O$ correlation using available stratospheric data. We included the CO_2 exchange fluxes from biosphere, oceans, and soils with the atmosphere. Also, we added the release of CO_2 to the atmosphere from fossil fuel combustion and biomass burning and the production of CO_2 through the oxidation of atmospheric CO.

Our 3-D model (with base model settings) predicts an average $\Delta^{17}O$ signature of 39.6 per meg for CO_2 in the lowest 500 m of the atmosphere, which is roughly 20 per meg lower than the prediction from the box model by Hofmann et al. (2017). This difference can be attributed mostly to the larger biosphere-atmosphere exchange in the 3-D model (global mean $F_{AL} = -514.5$ PgC/year for 2012/2013) compared to the box model ($F_{AL} = -352$ PgC/year) by Hofmann et al. (2017). For the NH and SH we predict a mean $\Delta^{17}O$ signature of 31.6 and 47.6 per meg, respectively. In addition, the $\Delta^{17}O$ signature exhibits a seasonal cycle with a peak-to-peak amplitude of 17.7 for the NH and 5.1 per meg for the SH, showing the largest drop in $\Delta^{17}O$ during the respective summer months for both hemispheres.

We showed that $\Delta^{17}O$ model predictions are sensitive to changes in the coefficients describing the N_2O–$\Delta^{17}O$ correlation for stratospheric CO_2. Also, the magnitude and spatial distribution of the soil invasion fluxes have a significant effect on $\Delta^{17}O$ in atmospheric CO_2. Furthermore, it was found that using a spatially explicit soil water signature $\Delta^{17}O_{soil}$ and time- and space-dependent leaf water signature $\Delta^{17}O_{leaf}$ has a limited effect on the resulting $\Delta^{17}O$ in atmospheric CO_2 and that the oxidation of CO has a minor effect on $\Delta^{17}O$ in atmospheric CO_2.

We compared our model predictions with a stratospheric profile of $\Delta^{17}O$ in CO_2 measured above Sodankylä, Finland (Mrozek et al., 2016), which showed good agreement indicating that our 3-D model is able to simulate these large-scale features of $\Delta^{17}O$ in atmospheric CO_2. Comparisons of model predictions with currently available tropospheric measurements of $\Delta^{17}O$ in CO_2 remain inconclusive due to the unexpected interannual variability for measurements from Göttingen, Germany (Hofmann et al., 2017) and the influence of local disturbances that cannot be resolved in our global model for Taipei, Taiwan (Liang & Mahata, 2015).

We identified Zotino, Russia (60.80°N, 89.35°E) as a suitable location to detect a large seasonal cycle of $\Delta^{17}O$ in CO_2 of 36.1 per meg, which is substantially larger than the uncertainty of several recently developed measurement techniques for $\Delta^{17}O$ in CO_2. Mauna Loa, USA (19.54°N, 155.58°W) and South Pole (90°S) are suitable background locations for which we predict a mean $\Delta^{17}O$ in CO_2 of 36.2 and 52.5 per meg respectively. For Manaus, Brazil (2.15°S, 59.00°W) we predict a small seasonal cycle in $\Delta^{17}O$ in CO_2 of 2.9 per meg but a strong vertical and longitudinal gradient. Measurements at the suggested locations or at comparable sites could help to further increase our understanding of the global $\Delta^{17}O$ budget for tropospheric CO_2.

Acknowledgments
We thank Thomas Launois for providing H_2 deposition maps. The European Research Council (ERC) is acknowledged for funding this research (649087) as part of the ASICA (Airborne Stable Isotopes of Carbon from the Amazon) project. The model simulations in this work have been performed using a grant for computing time (SH-312-14) from the Netherlands Organization for Scientific Research (NWO). The model output data that are used to produce the figures and tables in this paper are hosted by the ICOS Carbon Portal and are accessible online (https://doi.org/10.18160/3D4N-5YMF). We thank Kristie Boering and two anonymous reviewers for their constructive suggestions.

References

Adnew, G. A., Hofmann, M. E. G., Paul, D., Laskar, A., Surma, J., Albrecht, N., et al. (2019). Determination of the triple oxygen and carbon isotopic composition of CO_2 from atomic ion fragments formed in the ion source of the 253 Ultra High-Resolution Isotope Ratio Mass Spectrometer. *Rapid Communications in Mass Spectrometry*. https://doi.org/10.1002/rcm.8478

Affolter, S., Häuselmann, A. D., Fleitmann, D., Häuselmann, P., & Leuenberger, M. (2015). Triple isotope (δD, δ^{17}O, δ^{18}O) study on precipitation, drip water and speleothem fluid inclusions for a Western Central European cave (NW Switzerland). *Quaternary Science Reviews*, *127*, 73–89. https://doi.org/10.1016/j.quascirev.2015.08.030

Alexander, B., Vollmer, M. K., Jackson, T., Weiss, R. F., & Thiemens, M. H. (2001). Stratospheric CO_2 isotopic anomalies and SF_6 and CFC tracer concentrations in the Arctic polar vortex. *Geophysical Research Letters*, *28*(21), 4103–4106. https://doi.org/10.1029/2001GL013692

Andreae, M. O., Acevedo, O. C., Araùjo, A., Artaxo, P., Barbosa, C. G. G., Barbosa, H. M. J., et al. (2015). The Amazon Tall Tower Observatory (ATTO): Overview of pilot measurements on ecosystem ecology, meteorology, trace gases, and aerosols. *Atmospheric Chemistry and Physics*, *15*(18), 10,723–10,776. https://doi.org/10.5194/acp-15-10723-2015

Appenzeller, C., Holton, J. R., & Rosenlof, K. H. (1996). Seasonal variation of mass transport across the tropopause. *Journal of Geophysical Research*, *101*(D10), 15,071–15,078. https://doi.org/10.1029/96JD00821

Assonov, S. S., & Brenninkmeijer, C. A. M. (2003). A redetermination of absolute values for $^{17}R_{VPDB\text{-}CO2}$ and $^{17}R_{VSMOW}$. *Rapid Communications in Mass Spectrometry*, *17*(10), 1017–1029. https://doi.org/10.1002/rcm.1011

Assonov, S. S., Brenninkmeijer, C. A. M., Schuck, T., & Umezawa, T. (2013). N_2O as a tracer of mixing stratospheric and tropospheric air based on CARIBIC data with applications for CO_2. *Atmospheric Environment*, *79*, 769–779. https://doi.org/10.1016/j.atmosenv.2013.07.035

Baertschi, P. (1976). Absolute ^{18}O content of standard mean ocean water. *Earth and Planetary Science Letters*, *31*(3), 341–344. https://doi.org/10.1016/0012-821X(76)90115-1

Barkan, E., & Luz, B. (2012). High-precision measurements of $^{17}O/^{16}O$ and $^{18}O/^{16}O$ ratios in CO_2. *Rapid Communications in Mass Spectrometry*, *26*(23), 2733–2738. https://doi.org/10.1002/rcm.6400

Beer, C., Reichstein, M., Tomelleri, E., Ciais, P., Jung, M., Carvalhais, N., et al. (2010). Terrestrial gross carbon dioxide uptake: Global distribution and covariation with climate. *Science*, *329*(5993), 834–838. https://doi.org/10.1126/science.1184984

Bergamaschi, P., Corazza, M., Karstens, U., Athanassiadou, M., Thompson, R. L., Pison, I., et al. (2015). Top-down estimates of European CH_4 and N_2O emissions based on four different inverse models. *Atmospheric Chemistry and Physics*, *15*(2), 715–736. https://doi.org/10.5194/acp-15-715-2015

Boering, K. A., Jackson, T., Hoag, K. J., Cole, A. S., Perri, M. J., Thiemens, M., & Atlas, E. (2004). Observations of the anomalous oxygen isotopic composition of carbon dioxide in the lower stratosphere and the flux of the anomaly to the troposphere. *Geophysical Research Letters*, *31*, L03109. https://doi.org/10.1029/2003GL018451

Bönisch, H., Hoor, P., Gurk, C., Feng, W., Chipperfield, M., Engel, A., & Bregman, B. (2008). Model evaluation of CO_2 and SF_6 in the extratropical UT/LS region. *Journal of Geophysical Research*, *113*, D06101. https://doi.org/10.1029/2007JD008829

Booth, B. B. B., Jones, C. D., Collins, M., Totterdell, I. J., Cox, P. M., Sitch, S., et al. (2012). High sensitivity of future global warming to land carbon cycle processes. *Environmental Research Letters*, *7*(2), 024002. https://doi.org/10.1088/1748-9326/7/2/024002

Bowen, G. J., & Revenaugh, J. (2003). Interpolating the isotopic composition of modern meteoric precipitation. *Water Resources Research*, *39*(10), 1299. https://doi.org/10.1029/2003WR002086

Bregman, B., Meijer, E., & Scheele, R. (2006). Key aspects of stratospheric tracer modeling using assimilated winds. *Atmospheric Chemistry and Physics*, *6*(12), 4529–4543. https://doi.org/10.5194/acp-6-4529-2006

Brenninkmeijer, C. A. M., Kraft, P., & Mook, W. G. (1983). Oxygen isotope fractionation between CO_2 and H_2O. *Chemical Geology*, *41*, 181–190. https://doi.org/10.1016/S0009-2541(83)80015-1

Brenninkmeijer, C. A. M., Röckmann, T., Bräunlich, M., Jöckel, P., & Bergamaschi, P. (1999). Review of progress in isotope studies of atmospheric carbon monoxide. *Chemosphere - Global Change Science*, *1*(1-3), 33–52. https://doi.org/10.1016/S1465-9972(99)00018-5

Brühl, C., Steil, B., Stiller, G., Funke, B., & Jöckel, P. (2007). Nitrogen compounds and ozone in the stratosphere: Comparison of MIPAS satellite data with the chemistry climate model ECHAM5/MESSy1. *Atmospheric Chemistry and Physics*, *7*(21), 5585–5598. https://doi.org/10.5194/acp-7-5585-2007

Chakraborty, S., & Bhattacharya, S. K. (2003). Experimental investigation of oxygen isotope exchange between CO_2 and $O(^1D)$ and its relevance to the stratosphere. *Journal of Geophysical Research*, *108*(D23), 4724. https://doi.org/10.1029/2002JD002915

Ciais, P., Denning, A. S., Tans, P. P., Berry, J. A., Randall, D. A., Collatz, G. J., et al. (1997a). A three-dimensional synthesis study of $\delta^{18}O$ in atmospheric CO_2: 1. Surface fluxes. *Journal of Geophysical Research*, *102*(D5), 5857–5872. https://doi.org/10.1029/96JD02360

Ciais, P., Tans, P. P., Denning, A. S., Francey, R. J., Trolier, M., Meijer, H. A. J., et al. (1997b). A three-dimensional synthesis study of $\delta^{18}O$ in atmospheric CO_2: 2. Simulations with the TM2 transport model. *Journal of Geophysical Research*, *102*(D5), 5873–5883. https://doi.org/10.1029/96JD02361

Collatz, G. J., Ball, J. T., Grivet, C., & Berry, J. A. (1991). Physiological and environmental regulation of stomatal conductance, photosynthesis and transpiration: A model that includes a laminar boundary layer. *Agricultural and Forest Meteorology*, *54*(2-4), 107–136. https://doi.org/10.1016/0168-1923(91)90002-8

Collatz, G. J., Ribas-Carbo, M., & Berry, J. A. (1992). Coupled photosynthesis-stomatal conductance model for leaves of C_4 plants. *Australian Journal of Plant Physiology*, *19*(5), 519. https://doi.org/10.1071/PP9920519

Corazza, M., Bergamaschi, P., Vermeulen, A. T., Aalto, T., Haszpra, L., Meinhardt, F., et al. (2011). Inverse modelling of European N_2O emissions: Assimilating observations from different networks. *Atmospheric Chemistry and Physics*, *11*(5), 2381–2398. https://doi.org/10.5194/acp-11-2381-2011

Cuntz, M. (2011). A dent in carbon's gold standard. *Nature*, *477*(7366), 547–548. https://doi.org/10.1038/477547a

Cuntz, M., Ciais, P., & Hoffmann, G. (2002). Modelling the continental effect of oxygen isotopes over Eurasia. *Tellus B*, *54*(5), 895–911. https://doi.org/10.1034/j.1600-0889.2002.01341.x

Cuntz, M., Ciais, P., Hoffmann, G., Allison, C. E., Francey, R. J., Knorr, W., et al. (2003a). A comprehensive global three-dimensional model of $\delta^{18}O$ in atmospheric CO_2: 2. Mapping the atmospheric signal. *Journal of Geophysical Research*, *108*(D17), 4528. https://doi.org/10.1029/2002JD003154

Cuntz, M., Ciais, P., Hoffmann, G., & Knorr, W. (2003b). A comprehensive global three-dimensional model of $\delta^{18}O$ in atmospheric CO_2: 1. Validation of surface processes. *Journal of Geophysical Research*, *108*(D17), 4527. https://doi.org/10.1029/2002JD003153

DeMore, W. B., Sander, S. P., Golden, D. M., Hampson, R. F., Kurylo, M. J., Howard, C. J., et al. (1997). Chemical kinetics and photochemical data for use in stratospheric modeling (Evaluation Number 12, Tech. Rep.): Jet Propulsion Laboratory Pasadena California.

Dee, D. P., Uppala, S. M., Simmons, A. J., Berrisford, P., Poli, P., Kobayashi, S., et al. (2011). The ERA-Interim reanalysis: Configuration and performance of the data assimilation system. *Quarterly Journal of the Royal Meteorological Society*, *137*(656), 553–597. https://doi.org/10.1002/qj.828

Dubey, M. K., Mohrschladt, R., Donahue, N. M., & Anderson, J. G. (1997). Isotope specific kinetics of hydroxyl radical (OH) with water (H_2O): Testing models of reactivity and atmospheric fractionation. *The Journal of Physical Chemistry A*, *101*(8), 1494–1500. https://doi.org/10.1021/jp962332p

Dutkiewicz, V. A., & Husain, L. (1985). Stratospheric and tropospheric components of ^{7}Be in surface air. *Journal of Geophysical Research*, *90*(D3), 5783. https://doi.org/10.1029/JD090iD03p05783

Eiler, J. M., & Schauble, E. (2004). $^{18}O^{13}C^{16}O$ in Earth's atmosphere. *Geochimica et Cosmochimica Acta*, *68*(23), 4767–4777. https://doi.org/10.1016/j.gca.2004.05.035

Farquhar, G. D., Lloyd, J., Taylor, J. A., Flanagan, L. B., Syvertsen, J. P., Hubick, K. T., et al. (1993). Vegetation effects on the isotope composition of oxygen in atmospheric CO_2. *Nature*, *363*(6428), 439–443. https://doi.org/10.1038/363439a0

Farquhar, G. D., von Caemmerer, S., & Berry, J. A. (1980). A biochemical model of photosynthetic CO_2 assimilation in leaves of C_3 species. *Planta*, *149*(1), 78–90. https://doi.org/10.1007/BF00386231

Feilberg, K. L., Johnson, M. S., & Nielsen, C. J. (2005). Relative rates of reaction of $^{13}C^{16}O$, $^{12}C^{18}O$, $^{12}C^{17}O$ and $^{13}C^{18}O$ with OH and OD radicals. *Physical Chemistry Chemical Physics*, *7*(11), 2318. https://doi.org/10.1039/b503350k

Feilberg, K. L., Sellevåg, S. R., Nielsen, C. J., Griffith, D. W. T., & Johnson, M. S. (2002). $CO + OH \rightarrow CO_2, + H$: The relative reaction rate of five CO isotopologues. *Physical Chemistry Chemical Physics*, *4*(19), 4687–4693. https://doi.org/10.1039/B204827M

Francey, R. J., & Tans, P. P. (1987). Latitudinal variation in oxygen-18 of atmospheric CO_2. *Nature*, *327*(6122), 495–497. https://doi.org/10.1038/327495a0

Giglio, L., Randerson, J. T., & van der Werf, G. R. (2013). Analysis of daily, monthly, and annual burned area using the fourth-generation global fire emissions database (GFED4). *Journal of Geophysical Research: Biogeosciences*, *118*, 317–328. https://doi.org/10.1002/jgrg.20042

Gillon, J. S., & Yakir, D. (2000). Naturally low carbonic anhydrase activity in C_4 and C_3 plants limits discrimination against $C^{18}OO$ during photosynthesis, Plant. *Cell and Environment*, *23*(9), 903–915. https://doi.org/10.1046/j.1365-3040.2000.00597.x

Gillon, J., & Yakir, D. (2001). Influence of carbonic anhydrase activity in terrestrial vegetation on the ^{18}O content of atmospheric CO_2. *Science*, *291*(5513), 2584–2587. https://doi.org/10.1126/science.1056374

Gromov, S. S. (2013). Stable isotope composition of atmospheric carbon monoxide: A modelling study (Ph.D. thesis), Johannes Gutenberg-Universität Mainz. https://doi.org/10.13140/RG.2.2.30769.17760

Heimann, M., Schulze, E.-D., Winderlich, J., Andreae, M. O., Chi, X., Gerbig, C., et al. (2014). The Zotino Tall Tower Observatory (ZOTTO): Quantifying large scale biogeochemical changes in Central Siberia. *Nova Acta Leopoldina*, *117*(399), 51–64.

Hirsch, A. I., Michalak, A. M., Bruhwiler, L. M., Peters, W., Dlugokencky, E. J., & Tans, P. P. (2006). Inverse modeling estimates of the global nitrous oxide surface flux from 1998-2001. *Global Biogeochemical Cycles*, *20*, GB1008. https://doi.org/10.1029/2004GB002443

Hoag, K. J., Still, C. J., Fung, I. Y., & Boering, K. A. (2005). Triple oxygen isotope composition of tropospheric carbon dioxide as a tracer of terrestrial gross carbon fluxes. *Geophysical Research Letters*, *32*, L02802. https://doi.org/10.1029/2004GL021011

Hofmann, M. E. G., Horváth, B., Schneider, L., Peters, W., Schützenmeister, K., & Pack, A. (2017). Atmospheric measurements of $\Delta^{17}O$ in CO_2 in Göttingen, Germany reveal a seasonal cycle driven by biospheric uptake. *Geochimica et Cosmochimica Acta*, *199*, 143–163. https://doi.org/10.1016/j.gca.2016.11.019

Holloway, T., Levy, H., & Kasibhatla, P. (2000). Global distribution of carbon monoxide. *Journal of Geophysical Research*, *105*(D10), 12,123–12,147. https://doi.org/10.1029/1999JD901173

Holton, J. R. (1990). On the global exchange of mass between the stratosphere and troposphere. *Journal of the Atmospheric Sciences*, *47*(3), 392–395. https://doi.org/10.1175/1520-0469(1990)047<0392:OTGEOM>2.0.CO;2

Horváth, B., Hofmann, M. E. G., & Pack, A. (2012). On the triple oxygen isotope composition of carbon dioxide from some combustion processes. *Geochimica et Cosmochimica Acta*, *95*, 160–168. https://doi.org/10.1016/j.gca.2012.07.021

Huff, A. K., & Thiemens, M. H. (1998). $^{17}O/^{16}O$ and $^{18}O/^{16}O$ isotope measurements of atmospheric carbon monoxide and its sources. *Geophysical Research Letters*, *25*(18), 3509–3512. https://doi.org/10.1029/98GL02603

Huijnen, V., Williams, J., van Weele, M., van Noije, T., Krol, M., Dentener, F., et al. (2010). The global chemistry transport model TM5: Description and evaluation of the tropospheric chemistry version 3.0. *Geoscientific Model Development*, *3*(2), 445–473. https://doi.org/10.5194/gmd-3-445-2010

Jacobson, A. R., Mikaloff Fletcher, S. E., Gruber, N., Sarmiento, J. L., & Gloor, M. (2007). A joint atmosphere-ocean inversion for surface fluxes of carbon dioxide: 1. Methods and global-scale fluxes. *Global Biogeochemical Cycles*, *21*, GB1019. https://doi.org/10.1029/2005GB002556

Johnston, J. C., Röckmann, T., & Brenninkmeijer, C. A. M. (2000). CO_2 + $O(^1D)$ isotopic exchange: Laboratory and modeling studies. *Journal of Geophysical Research*, *105*(D12), 15,213–15,229. https://doi.org/10.1029/2000JD900070

Kaiser, J. (2008). Reformulated ^{17}O correction of mass spectrometric stable isotope measurements in carbon dioxide and a critical appraisal of historic 'absolute' carbon and oxygen isotope ratios. *Geochimica et Cosmochimica Acta*, *72*(5), 1312–1334. https://doi.org/10.1016/j.gca.2007.12.011

Kawagucci, S., Tsunogai, U., Kudo, S., Nakagawa, F., Honda, H., Aoki, S., et al. (2008). Long-term observation of mass-independent oxygen isotope anomaly in stratospheric CO_2. *Atmospheric Chemistry and Physics*, *8*(20), 6189–6197. https://doi.org/10.5194/acp-8-6189-2008

Krol, M., Houweling, S., Bregman, B., van den Broek, M., Segers, A., van Velthoven, P., et al. (2005). The two-way nested global chemistry-transport zoom model TM5: Algorithm and applications. *Atmospheric Chemistry and Physics*, *5*(2), 417–432. https://doi.org/10.5194/acp-5-417-2005

Lämmerzahl, P., Röckmann, T., Brenninkmeijer, C. A. M., Krankowsky, D., & Mauersberger, K. (2002). Oxygen isotope composition of stratospheric carbon dioxide. *Geophysical Research Letters*, *29*(12), 1582. https://doi.org/10.1029/2001GL014343

Landais, A., Barkan, E., Yakir, D., & Luz, B. (2006). The triple isotopic composition of oxygen in leaf water. *Geochimica et Cosmochimica Acta*, *70*(16), 4105–4115. https://doi.org/10.1016/j.gca.2006.06.1545

Laskar, A. H., Mahata, S., Bhattacharya, S. K., & Liang, M.-C. (2019). Triple oxygen and clumped isotope compositions of CO2 in the middle troposphere. *Earth and Space Science*, *6*. https://doi.org/10.1029/2019EA000573.

Laskar, A. H., Mahata, S., & Liang, M.-C. (2016). Identification of anthropogenic CO_2 using triple oxygen and clumped isotopes. *Environmental Science & Technology*, *50*(21), 11,806–11,814. https://doi.org/10.1021/acs.est.6b02989

Launois, T., Peylin, P., Belviso, S., & Poulter, B. (2015). A new model of the global biogeochemical cycle of carbonyl sulfide Part 2: Use of carbonyl sulfide to constrain gross primary productivity in current vegetation models. *Atmospheric Chemistry and Physics*, *15*(16), 9285–9312. https://doi.org/10.5194/acp-15-9285-2015

Li, W., Ni, B., Deqiu, J., & Qinglian, Z. (1988). Measurement of the absolute abundance of oxygen-17 in V-SMOW. *Chinese Science Bulletin*, *33*(19), 1610–1613.

Liang, M.-C., Blake, G. A., Yung, Y. L., (2008) Seasonal cycle of $C^{16}O^{16}O$, $C^{16}O^{17}O$, and $C^{16}O^{18}O$ in the middle atmosphere: Implications for mesospheric dynamics and biogeochemical sources and sinks of CO_2. *Journal of Geophysical Research*, *113*, D12305. https://doi.org/10.1029/2007JD008392

Liang, M.-C., & Mahata, S. (2015). Oxygen anomaly in near surface carbon dioxide reveals deep stratospheric intrusion. *Scientific Reports*, *5*(11), 352. https://doi.org/10.1038/srep11352

Liang, M.-C., Mahata, S., Laskar, A. H., & Bhattacharya, S. K. (2017a). Spatiotemporal variability of oxygen isotope anomaly in near surface air CO_2 over urban, semi-urban and ocean areas in and around Taiwan. *Aerosol and Air Quality Research*, *17*(3), 706–720. https://doi.org/10.4209/aaqr.2016.04.0171

Liang, M.-C., Mahata, S., Laskar, A. H., Thiemens, M. H., & Newman, S. (2017b). Oxygen isotope anomaly in tropospheric CO_2 and implications for CO_2 residence time in the atmosphere and gross primary productivity. *Scientific Reports*, *7*(1), 13180. https://doi.org/10.1038/s41598-017-12774-w

Luz, B., & Barkan, E. (2010). Variations of $^{17}O/^{16}O$ and $^{18}O/^{16}O$ in meteoric waters. *Geochimica et Cosmochimica Acta*, *74*(22), 6276–6286. https://doi.org/10.1016/j.gca.2010.08.016

Luz, B., Barkan, E., Bender, M. L., Thiemens, M. H., & Boering, K. A. (1999). Triple-isotope composition of atmospheric oxygen as a tracer of biosphere productivity. *Nature*, *400*(6744), 547–550. https://doi.org/10.1038/22987

Lyons, J. R. (2001). Transfer of mass-independent fractionation in ozone to other oxygen-containing radicals in the atmosphere. *Geophysical Research Letters*, *28*(17), 3231–3234. https://doi.org/10.1029/2000GL012791

Mahata, S., Bhattacharya, S. K., & Liang, M.-C. (2016b). An improved method of high-precision determination of $\Delta^{17}O$ of CO_2 by catalyzed exchange with O_2 using hot platinum. *Rapid Communications in Mass Spectrometry*, *30*(1), 119–131. https://doi.org/10.1002/rcm.7423

Mahata, S., Bhattacharya, S. K., Wang, C.-H., & Liang, M.-C. (2013). Oxygen isotope exchange between O_2 and CO_2 over hot platinum: An innovative technique for measuring $\Delta^{17}O$ in CO_2. *Analytical Chemistry*, *85*(14), 6894–6901. https://doi.org/10.1021/ac4011777

Mahata, S., Wang, C.-H., Bhattacharya, S. K., & Liang, M.-C. (2016a). Near surface CO_2 triple oxygen isotope composition. *Terrestrial, Atmospheric and Oceanic Sciences*, *27*(1), 99–106. https://doi.org/10.3319/TAO.2015.09.16.01(A)

McManus, J. B., Nelson, D. D., & Zahniser, M. S. (2015). Design and performance of a dual-laser instrument for multiple isotopologues of carbon dioxide and water. *Optics Express*, *23*(5), 6569. https://doi.org/10.1364/OE.23.006569

Mebel, A. M., Hayashi, M., Kislov, V. V., & Lin, S. H. (2004). Theoretical study of oxygen isotope exchange and quenching in the $O(^1D)$ + CO_2 reaction. *The Journal of Physical Chemistry A*, *108*(39), 7983–7994. https://doi.org/10.1021/jp049315h

Miller, J. B., Yakir, D., White, J. W. C., & Tans, P. P. (1999). Measurement of $^{18}O/^{16}O$ in the soil-atmosphere CO_2 flux. *Global Biogeochemical Cycles*, *13*(3), 761–774. https://doi.org/10.1029/1999GB900028

Monge-Sanz, B. M., Chipperfield, M. P., Simmons, A. J., & Uppala, S. M. (2007). Mean age of air and transport in a CTM: Comparison of different ECMWF analyses. *Geophysical Research Letters*, *34*, L04801. https://doi.org/10.1029/2006GL028515

Mrozek, D. J. (2017). Measurements and interpretation of oxygen isotopes in stratospheric carbon dioxide (Ph.D. thesis), Utrecht University.

Mrozek, D. J., van der Veen, C., Hofmann, M. E. G., Chen, H., Kivi, R., Heikkinen, P., & Röckmann, T. (2016). Stratospheric Air Sub-sampler (SAS) and its application to analysis of $\Delta^{17}O(CO_2)$ from small air samples collected with an AirCore. *Atmospheric Measurement Techniques*, *9*(11), 5607–5620. https://doi.org/10.5194/amt-9-5607-2016

Nelson, D. D., McManus, J. B., Herndon, S. C., Zahniser, M. S., Tuzson, B., & Emmenegger, L. (2008). New method for isotopic ratio measurements of atmospheric carbon dioxide using a 4.3 μm pulsed quantum cascade laser. *Applied Physics B*, *90*(2), 301–309. https://doi.org/10.1007/s00340-007-2894-1

Ogée, J., Sauze, J., Kesselmeier, J., Genty, B., Van Diest, H., Launois, T., & Wingate, L. (2016). A new mechanistic framework to predict OCS fluxes from soils. *Biogeosciences*, *13*(8), 2221–2240. https://doi.org/10.5194/bg-13-2221-2016

Oort, A. H. (1983). Global atmospheric circulation statistics, 1958-1973. U.S, Department of Commerce National Oceanic and Atmospheric Administration.

Pearcy, R. W., & Ehleringer, J. (1984). Comparative ecophysiology of C_3 and C_4 plants. *Plant Cell and Environment*, *7*(1), 1–13. https://doi.org/10.1111/j.1365-3040.1984.tb01194.x

Peters, W., Jacobson, A. R., Sweeney, C., Andrews, A. E., Conway, T. J., Masarie, K., et al. (2007). An atmospheric perspective on North American carbon dioxide exchange: CarbonTracker. *Proceedings of the National Academy of Sciences*, *104*(48), 18,925–18,930. https://doi.org/10.1073/pnas.0708986104

Peters, W., Krol, M. C., van der Werf, G. R., Houweling, S., Jones, C. D., Hughes, J., et al. (2010). Seven years of recent European net terrestrial carbon dioxide exchange constrained by atmospheric observations. *Global Change Biology*, *16*(4), 1317–1337. https://doi.org/10.1111/j.1365-2486.2009.02078.x

Peters, W., van der Velde, I. R., van Schaik, E., Miller, J. B., Ciais, P., Duarte, H. F., et al. (2018). Increased water-use efficiency and reduced CO_2 uptake by plants during droughts at a continental scale. *Nature Geoscience*, *11*(10), 744–748. https://doi.org/10.1038/s41561-018-0212-7

Peylin, P., Ciais, P., Denning, A. S., Tans, P. P., Berry, J. A., & White, J. W. C. (1999). A 3-dimensional study of $\delta^{18}O$ in atmospheric CO_2: Contribution of different land ecosystems. *Tellus B*, *51*(3), 642–667. https://doi.org/10.1034/j.1600-0889.1999.t01-2-00006.x

Peylin, P., Ciais, P., Tans, P. P., Six, K., Berry, J. A., & Denning, A. S. (1997). ^{18}O in atmospheric CO_2 simulated by a 3-D transport model: A sensitivity study to vegetation and soil fractionation factors. *Physics and Chemistry of the Earth*, *21*(5-6), 463–469. https://doi.org/10.1016/S0079-1946(97)81143-3

Potter, C. S., Randerson, J. T., Field, C. B., Matson, P. A., Vitousek, P. M., Mooney, H. A., & Klooster, S. A. (1993). Terrestrial ecosystem production: A process model based on global satellite and surface data. *Global Biogeochemical Cycles*, *7*(4), 811–841. https://doi.org/10.1029/93GB02725

Prather, M. J. (1986). Numerical advection by conservation of second-order moments. *Journal of Geophysical Research*, *91*(D6), 6671. https://doi.org/10.1029/JD091iD06p06671

Röckmann, T., Brenninkmeijer, C. A. M., Neeb, P., & Crutzen, P. J. (1998b). Ozonolysis of nonmethane hydrocarbons as a source of the observed mass independent oxygen isotope enrichment in tropospheric CO. *Journal of Geophysical Research*, *103*(D1), 1463–1470. https://doi.org/10.1029/97JD02929

Röckmann, T., Brenninkmeijer, C. A. M., Saueressig, G., Bergamaschi, P., Crowley, J. N., Fischer, H., & Crutzen, P. J. (1998a). Mass-independent oxygen isotope fractionation in atmospheric CO as a result of the reaction CO + OH. *Science*, *281*(5376), 544–546. https://doi.org/10.1126/science.281.5376.544

Röckmann, T., Jöckel, P., Gros, V., Bräunlich, M., Possnert, G., & Brenninkmeijer, C. A. M. (2002). Using ^{14}C, ^{13}C, ^{18}O and ^{17}O isotopic variations to provide insights into the high northern latitude surface CO inventory. *Atmospheric Chemistry and Physics*, *2*(2), 147–159. https://doi.org/10.5194/acp-2-147-2002

Russell, G. L., & Lerner, J. A. (1981). A new finite-differencing scheme for the tracer transport equation. *Journal of Applied Meteorology*, *20*(12), 1483–1498. https://doi.org/10.1175/1520-0450(1981)020<1483:ANFDSF>2.0.CO;2

Sanhueza, E., Dong, Y., Lobert, J. M., & Crutzen, P. J. (1998). Carbon monoxide uptake by temperate forest soils: The effects of leaves and humus layers. *Tellus B*, *50*(1), 51–58. https://doi.org/10.1034/j.1600-0889.1998.00004.x

Schaefer, K., Collatz, G. J., Tans, P., Denning, A. S., Baker, I., Berry, J., et al. (2008). Combined Simple Biosphere/Carnegie-Ames-Stanford Approach terrestrial carbon cycle model. *Journal of Geophysical Research*, *113*, G03034. https://doi.org/10.1029/2007JG000603

Schoeberl, M. R., Douglass, A. R., Stolarski, R. S., Pawson, S., Strahan, S. E., & Read, W. (2008). Comparison of lower stratospheric tropical mean vertical velocities. *Journal of Geophysical Research*, *113*, D24109. https://doi.org/10.1029/2008JD010221

Shaheen, R., Janssen, C., & Röckmann, T. (2007). Investigations of the photochemical isotope equilibrium between O_2, CO_2 and O_3. *Atmospheric Chemistry and Physics*, *7*(2), 495–509. https://doi.org/10.5194/acp-7-495-2007

Spivakovsky, C. M., Logan, J. A., Montzka, S. A., Balkanski, Y. J., Foreman-Fowler, M., Jones, D. B. A., et al. (2000). Three-dimensional climatological distribution of tropospheric OH: Update and evaluation. *Journal of Geophysical Research*, *105*(D7), 8931–8980. https://doi.org/10.1029/1999JD901006

Stern, L. A., Amundson, R., & Baisden, W. T. (2001). Influence of soils on oxygen isotope ratio of atmospheric CO_2. *Global Biogeochemical Cycles*, *15*(3), 753–759. https://doi.org/10.1029/2000GB001373

Still, C. J., Berry, J. A., Collatz, G. J., & DeFries, R. S. (2003). Global distribution of C_3 and C_4 vegetation: Carbon cycle implications. *Global Biogeochemical Cycles*, *17*(1), 1006. https://doi.org/10.1029/2001GB001807

Stoltmann, T., Casado, M., Daëron, M., Landais, A., & Kassi, S. (2017). Direct, precise measurements of isotopologue abundance ratios in CO_2 using molecular absorption spectroscopy: Application to $\Delta^{17}O$. *Analytical Chemistry*, *89*(19), 10,129–10,132. https://doi.org/10.1021/acs.analchem.7b02853

Swinbank, R., & O'Neill, A. (1994). A stratosphere-troposphere data assimilation system. *Monthly Weather Review*, *122*(4), 686–702. https://doi.org/10.1175/1520-0493(1994)122<0686:ASTDAS>2.0.CO;2

Thiemens, M. H., Chakraborty, S., & Jackson, T. L. (2014). Decadal $\Delta^{17}O$ record of tropospheric CO_2: Verification of a stratospheric component in the troposphere. *Journal of Geophysical Research: Atmospheres*, *119*, 6221–6229. https://doi.org/10.1002/2013JD020317

Thiemens, M. H., Jackson, T. L., & Brenninkmeijer, C. A. M. (1995b). Observation of a mass independent oxygen isotopic composition in terrestrial stratospheric CO_2, the link to ozone chemistry, and the possible occurrence in the Martian atmosphere. *Geophysical Research Letters*, *22*(3), 255–257. https://doi.org/10.1029/94GL02996

Thiemens, M. H., Jackson, T., Zipf, E. C., Erdman, P. W., & van Egmond, C. (1995a). Carbon dioxide and oxygen isotope anomalies in the mesosphere and stratosphere. *Science*, *270*(5238), 969–972. https://doi.org/10.1126/science.270.5238.969

Tian, C., Wang, L., Kaseke, K. F., & Bird, B. W. (2018). Stable isotope compositions (δ^2H, $\delta^{18}O$ and $\delta^{17}O$) of rainfall and snowfall in the central United States. *Scientific Reports*, *8*(1), 6712. https://doi.org/10.1038/s41598-018-25102-7

Uemura, R., Barkan, E., Abe, O., & Luz, B. (2010). Triple isotope composition of oxygen in atmospheric water vapor. *Geophysical Research Letters*, *37*, L04402. https://doi.org/10.1029/2009GL041960

van Noije, T. P. C., Eskes, H. J., van Weele, M., & van Velthoven, P. F. J. (2004). Implications of the enhanced Brewer-Dobson circulation in European Centre for Medium-Range Weather Forecasts reanalysis ERA-40 for the stratosphere-troposphere exchange of ozone in global chemistry transport models. *Journal of Geophysical Research*, *109*, D19308. https://doi.org/10.1029/2004JD004586

van der Laan-Luijkx, I. T., van der Velde, I. R., van der Veen, E., Tsuruta, A., Stanislawska, K., Babenhauserheide, A., et al. (2017). The CarbonTracker Data Assimilation Shell (CTDAS) v1.0: Implementation and global carbon balance 2001-2015. *Geoscientific Model Development*, *10*(7), 2785–2800. https://doi.org/10.5194/gmd-10-2785-2017

van der Velde, I. R., Miller, J. B., Schaefer, K., van der Werf, G. R., Krol, M. C., & Peters, W. (2014). Terrestrial cycling of $^{13}CO_2$ by photosynthesis, respiration, and biomass burning in SiBCASA. *Biogeosciences*, *11*(23), 6553–6571. https://doi.org/10.5194/bg-11-6553-2014

van der Werf, G. R., Randerson, J. T., Giglio, L., Collatz, G. J., Mu, M., Kasibhatla, P. S., et al. (2010). Global fire emissions and the contribution of deforestation, savanna, forest, agricultural, and peat fires (1997-2009). *Atmospheric Chemistry and Physics*, *10*(23), 11,707–11,735. https://doi.org/10.5194/acp-10-11707-2010

Vilà-Guerau de Arellano, J., Koren, G., Ouwersloot, H. G., van der Velde, I., Röckmann, T., & Miller, J. B. (2019). Sub-diurnal variability of the carbon dioxide and water vapor isotopologues at the field observational scale. *Agricultural and Forest Meteorology*, *275*, 114–135. https://doi.org/10.1016/j.agrformet.2019.05.014

Vogel, J. C., Grootes, P. M., & Mook, W. G. (1970). Isotopic fractionation between gaseous and dissolved carbon dioxide. *Zeitschrift für Physik A Hadrons and nuclei*, *230*(3), 225–238. https://doi.org/10.1007/BF01394688

Volk, C. M., Elkins, J. W., Fahey, D. W., Dutton, G. S., Gilligan, J. M., Loewenstein, M., et al. (1997). Evaluation of source gas lifetimes from stratospheric observations. *Journal of Geophysical Research*, *102*(D21), 25,543–25,564. https://doi.org/10.1029/97JD02215

Wanninkhof, R. (1992). Relationship between wind speed and gas exchange over the ocean. *Journal of Geophysical Research*, *97*(C5), 7373. https://doi.org/10.1029/92JC00188

Welp, L. R., Keeling, R. F., Meijer, H. A. J., Bollenbacher, A. F., Piper, S. C., Yoshimura, K., et al. (2011). Interannual variability in the oxygen isotopes of atmospheric CO_2 driven by El Niño. *Nature*, *477*(7366), 579–582. https://doi.org/10.1038/nature10421

Wen, J., & Thiemens, M. H. (1993). Multi-isotope study of the $O(^1D)$ + CO_2 exchange and stratospheric consequences. *Journal of Geophysical Research*, *98*(D7), 12,801–12,808. https://doi.org/10.1029/93JD00565

West, J. B., Sobek, A., & Ehleringer, J. R. (2008). A simplified GIS approach to modeling global leaf water isoscapes. *PLoS ONE*, *3*(6), e2447. https://doi.org/10.1371/journal.pone.0002447

Wiegel, A. A., Cole, A. S., Hoag, K. J., Atlas, E. L., Schauffler, S. M., & Boering, K. A. (2013). Unexpected variations in the triple oxygen isotope composition of stratospheric carbon dioxide. *Proceedings of the National Academy of Sciences*, *110*(44), 17,680–17,685. https://doi.org/10.1073/pnas.1213082110

Wingate, L., Ogée, J., Cuntz, M., Genty, B., Reiter, I., Seibt, U., et al. (2009). The impact of soil microorganisms on the global budget of ^{18}O in atmospheric CO_2. *Proceedings of the National Academy of Sciences*, *106*(52), 22,411–22,415. https://doi.org/10.1073/pnas.0905210106

Yeung, L. Y., Affek, H. P., Hoag, K. J., Guo, W., Wiegel, A. A., Atlas, E. L., et al. (2009). Large and unexpected enrichment in stratospheric $^{16}O^{13}C^{18}O$ and its meridional variation. *Proceedings of the National Academy of Sciences*, *106*(28), 11,496–11,501. https://doi.org/10.1073/pnas.0902930106

Young, E. D., Galy, A., & Nagahara, H. (2002). Kinetic and equilibrium mass-dependent isotope fractionation laws in nature and their geochemical and cosmochemical significance. *Geochimica et Cosmochimica Acta*, *66*(6), 1095–1104. https://doi.org/10.1016/S0016-7037(01)00832-8

Yung, Y. L., DeMore, W. B., & Pinto, J. P. (1991). Isotopic exchange between carbon dioxide and ozone via $O(^1D)$ in the stratosphere. *Geophysical Research Letters*, *18*(1), 13–16. https://doi.org/10.1029/90GL02478